ETH
Eidgenössische Technische Hochschule Zürich
Swiss Federal Institute of Technology Zurich

KIT
Karlsruher Institut für Technologie

May-Oct 2016 Prof. Dr. Sebastian Huber

Master's Thesis

Cavity QED meets Bose-Einstein condensate: theoretical studies of their dynamics

Chiara Decaroli

Advisors: Prof. Dr. Sebastian Huber
Prof. Dr. Carsten Rockstuhl
Prof. Dr. Tilman Esslinger
Dr. Tobias Donner

Acknowledgments

I would like to sincerely thank my main supervisor Prof. Sebastian Huber, first of all for having given me the opportunity to carry out a thesis in theoretical Physics despite my prevalently experimental background. Secondly for his guidance and mentoring during the months I spent at ETH. I also deeply appreciated the freedom and pace of the project, which taught me many lessons about independent work and self confidence. I also thank him for allowing me to carry out research on interesting and engaging topics and for always finding some time for me despite a very busy schedule.

I would like to thank Tobias Donner and Tilman Esslinger for the numerous meetings during which the direction of the project was defined and the Physics interpretations were discussed. I feel very privileged to have had exposure to such skilled and high level researchers and I hope to have learnt many things about "thinking and doing Physics" from these meetings.

I thank Evert, Sina, Roman and Andrea for useful discussions about the thesis projects.

I kindly thank the QSIT Network for granting me the INSPIRE scholarship which allowed me to sustain myself financially independently from my parents during the thesis.

Finally I would like to thank my KSOP co-supervisor, Carsten Rocksthul, for his support and presence during the period of the thesis and for having accepted to be my thesis supervisor within my Europhotonics Master Programme.

Declaration

Ich versichere wahrheitsgemäß, die Arbeit selbstständig verfasst, alle benutzten Hilfsmittel vollständig und genau angegeben und alles kenntlich gemacht zu haben, was aus Arbeiten anderer unverändert oder mit Abänderungen entnommen wurde sowie die Satzung des KIT KSOP SPO 2015 English 18 zur Sicherung guter wissenschaftlicher Praxis in der jeweils gültigen Fassung beachtet zu haben. (I herewith declare that the present thesis is original work written by me alone, that I have indicated completely and precisely all aids used as well as all citations, whether changed or unchanged, of other theses and publications, and that I have observed the KIT Statutes for Upholding Good Scientific Practice, as amended).

Karlsruhe, 25th October 2016

Chiara Decaroli

Abstract

This theoretical work stems from a collaboration with Tilman Esslinger's experimental quantum optics group at ETH. Two main research directions are explored, both strongly linked and motivated by recent experimental achievements.

The former focuses on the cavity experiment, in which a ^{87}Rb BEC is confined in an optical lattice and embedded in an ultrahigh finesse cavity orthogonal to the pump laser. The interaction between the pump laser, the cavity mode and the BEC atoms gives birth to a plethora of fascinating phenomena and dynamics [1]. The novelty of this setup is the presence of the ultrahigh finesse cavity, which, via off resonant scattering, mediates long range interactions. The Hamiltonian describing the system is not any longer the usual Bose-Hubbard Hamiltonian but it also includes an additional long range interaction term. We are interested in studying the impact of this long range term on the dynamics of the condensate. Motivated by the results for a case without long range interactions [2], we aim at extending this model. We construct a simulation for a system of four sites and two atoms per site and evolve the matter wave function in the Heisenberg picture. We show that the dynamics persists for commensurate values of the interactions strengths and characterise the revival time for experimental values of these quantities. We propose this measurement of the dynamics as a pump-probe method to quantify with precision the long range interactions present in the system.

The second half of this work focuses on the IMPACT experiment [3], where a BEC is now positioned within two cavities at 60° angle to the pump. Here, we are interested in calculating the band structure for the resulting optical potential. We adapt former Python scripts in order to compute the lower energy bands of the system. We analyse all the possible scattering events and the Hamiltonian for the system, towards the implementation of the calculation of the bands.

Keywords BEC, Cavity QED, Collapse and Revivals, Extended Bose Hubbard model, Heisenberg picture, Coherent states, Band structure, Hamiltonian, Optical potential, Scattering

Contents

Chapter 1

Setting the scene

Nature isn't classical ... and if you want to make a simulation of Nature, you'd better make it quantum mechanical, and by golly it's a wonderful problem, because it doesn't look so easy.

R. P. Feynman, 1981

1.1 Quantum simulation

The proposal of the first Quantum Computer was put forward by Richard Feynman in 1982 [4]. Back then, Feynman had the brilliant idea of focusing the attention on simulating physical systems. However, he was well aware of the inherent quantum nature of reality, therefore he proposed an entirely new machine, a quantum computer, capable of imitating in all ways a quantum system and therefore able to simulate it accurately.

A decade later, in 1996, Seth Lloyd published a paper entitled "Universal Quantum Simulators". Its abstract reads: "Feynman's 1982 conjecture, that quantum computers can be programmed to simulate any local quantum system, is shown to be correct." [5] . These two papers marked the birth of the field of Quantum Simulation. Quantum simulators have since been under the spotlight due to their computational capabilities [6]. Quantum simulators are systems whose properties are very well known and kept under control, for this reason they can be used to sim-

ulate with incredible precision real quantum systems [7]. This of course represents a remarkable potential for deeper understanding, particularly in a time when more and more quantum phenomena are exploited in our technology and when there are several problems which we cannot address completely with our current classical computational architectures.

A wide collection of physical systems was proposed as quantum simulators such as: ultracold quantum gases, trapped ions, quantum dots, photonic systems and superconducting qubits [8]. These systems had two main objectives: being able to reproduce with high precision a specific Hamiltonian in order to address problems which are not tractable in the laboratory, and being able to solve problems which are not accessible via classical computations. Complex quantum ground states and dynamics of solid state systems fall in the latter category. Indeed solid state physics is incredibly rich in problems which are currently not solvable using classical computation due to the high number of particles involved in the problem. To mention a few examples of challenges which are posed by solid state physics and which are being investigated by quantum simulators: spin-boson models, 1D [9] and 2D systems [10], Kondo physics [11], Hubbard and spin models [12], disordered systems [13], high T_c superconductivity, topological order [14], fractional quantum Hall states, and many more [15].

Thanks to the technical advances in the field in the last decades, the level of quantum engineering involved has reached unprecedented peaks, allowing for precision control and measurement of quantum systems [16]. Seminal discoveries in this direction have been the cooling and trapping of atoms, ions and molecules [17], where physics phenomena were until then unaccessible; laser cooling and evaporative cooling, which allowed the first experimental observations of a BEC [18], [19]; a better understanding of quantum correlations and entanglement; optical lattices and Feshback resonances, which increased the control capability and the ability to create lattices resembling those in solid state physics. Almost twenty years after the first experimental discoveries, the field of quantum simulation is rich in results and yet still rich in questions to be answered [20].

In the following work we will restrict our interest to a specific type of quantum simulations: namely quantum simulation with Bose Einstein condensation (BEC) confined in an optical cavity. We will express the reason for using an optical res-

onator and the advantages which derive from it, hence we will conclude this introduction by describing the two experiments on which this work is based.

1.1.1 Quantum simulation with BEC in optical cavities

Light matter interactions are one of the most fundamental and fascinating phenomena in nature. If we consider a single two level atom irradiated by a light field with the frequency of the light far detuned from the resonant frequency of the atomic transition between the ground and excited level, spontaneous emission is suppressed and coherent scattering of photons is predominant, resulting in the optical dipole force. In a free space situation, the back action of the particle on the light is negligible, *i.e.* the particle does not detect a modification of the light field and the light field can be considered a conservative optical potential [21].

However, when the system is embedded in a high finesse cavity, the photons circle inside the resonator resulting in an enhancement of the dipole force and producing remarkable back action on the light field. In this scenario the atomic motion and the cavity field dynamics continuously influence one another. From this new dynamics regime interference effect and self organising phases arise. Moreover, the cavity represents an open system, photons leak out of the cavity and allow for a real time monitoring tool.

Self organisation effects in the cavity lead to the formation of dynamical superlattices and as a result long range interactions among the atoms are mediated by the cavity field. This gives the possibility of engineering tailored long range interactions between atoms, which is not possible in free space cold atoms experiments [22].

The following paragraph will present the theory of the Jaynes-Cummings model and the Tavis-Cummings model, which are at the backbone of this work.

1.1.2 Cavity QED and the Cummings models

In the attempt of understanding the interaction between light and matter in this scenario, and how the presence of the cavity affects the resulting dynamics, we consider a two level system in a cavity and an electromagnetic field impinging on it [23], [24]. Light matter interaction can manifest itself in three ways: absorption, spontaneous emission and stimulated emission.

In some cases, the absorption can be virtual, resulting in the re-emission of a photon of the same colour as the incoming photon but in a random direction. This is the case of a radiation field which is far detuned with respect to the atomic resonance transition. The interaction is coherent and it results in the scattering of the photons off the atoms. Due to conservation of momentum, the atoms receive a recoil kick and move away from their original position. This change in the position of the atom has an effect on the perceived electric dipole force from the radiation field. However, when in free space, this perceived shift is negligible.

The effect becomes substantial when the atom and the field are enclosed in an optical cavity. Optical cavities have the aim of enhancing the interaction between light and matter. They are closed systems in which light bounces off mirrors and travels several time along the same path. In a simple Fabry-Perot cavity, two curved mirrors with reflectivity R, face each other. The light bounces back and forth, with power enhancement factor of F/π, where F is the finesse of the cavity and it is given by $F = \frac{\pi\sqrt{R}}{1-R}$. The probability to scatter a photon on a single atom is give by a quantity called the cooperativity $C = \sigma/A$ in free space, where σ is the scattering cross section and A the area of the laser beam. In a resonator, the cooperativity is enhanced to $C = \frac{F\sigma}{\pi A}$, for more than one atom this becomes $C = N\frac{F\sigma}{\pi A}$.

When the cooperativity is greater than 1, there will be a substantial backaction of the atoms on the light field. As the photons scatter off the atoms, the atoms experience a recoil and move, this motion influences the light field in return and therefore modifies the light potential dynamically. The optical potential is not static anymore, and even a single photon can create a potential strong enough to influence the atoms.

The picture of a single atom interacting with a single mode of an electromagnetic field is described by the Jaynes-Cummings Hamiltonian. According to the Jaynes-Cummings model, the system is described by the Hamiltonian given below, made up of three components. The three components refer respectively to the atomic Hamiltonian, the electromagnetic field Hamiltonian and the interaction Hamiltonian between atom and field. The Jaynes Cummings model is a quantum model of the interaction of light and matter, this implies that not only the atom is a quantum mechanical object, but also the electromagnetic field is quantised. It is

slightly modified when considering the interaction between a single atom and a single mode of the field of a cavity by adding a term describing the field pumping the cavity. In the following, we will consider a pump parallel to the cavity direction. The Jaynes Cummings Hamitonian is given by:

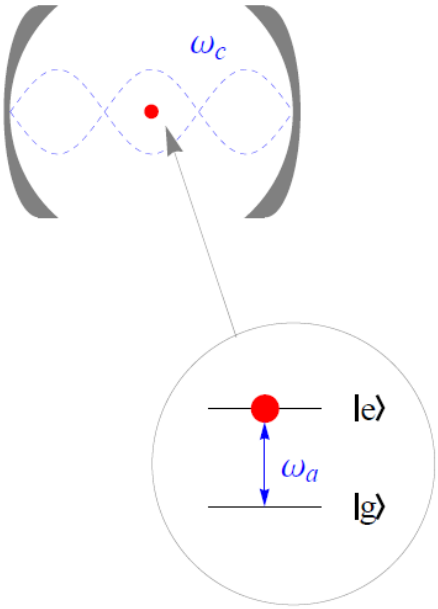

Figure 1.1: Illustration of the Jaynes Cummings model. A two level atom in a cavity interacts with a light field. ω_{a} and ω_{c} represent the resonance frequencies of the light and the atomic transition.

$$H_{\mathrm{JC}} = H_{\mathrm{atom}} + H_{\mathrm{field}} + H_{\mathrm{interaction}}. \tag{1.1}$$

Let us study in detail each one of these terms. The first term of the equation refers to the atomic Hamiltonian, and, considering both internal and external degrees of freedom, is given by:

$$H_{\mathrm{atom}} = \frac{p^2}{2m} + V_{\mathrm{ext}}(x) + \hbar\omega_{\mathrm{a}}\hat{\sigma}_z, \tag{1.2}$$

here, the first two terms describe the kinetic energy of the atom and an external potential, the third term describes the excitation energy of the two level system, modelled as a spin-1/2 particle with ground state $|g\rangle$ and excited state $|e\rangle$. In this picture, the two level atom lives in a Hilbert space spanned by two energy eigenstates, *i.e.* the 2D Hilbert space is equivalent to that of a spin-1/2 particle and

can be thought of as a 2-vector: $\alpha\,|e\rangle + \beta\,|g\rangle = \begin{pmatrix} \alpha \\ \beta \end{pmatrix}$. Transitions between the two levels are given by the Pauli matrices $\hat{\sigma}_{\mathrm{x}}$, $\hat{\sigma}_{\mathrm{y}}$ and $\hat{\sigma}_{\mathrm{z}}$, and their superpositions $\hat{\sigma}_+$ = 1/2($\hat{\sigma}_{\mathrm{x}} + i\hat{\sigma}_{\mathrm{y}}$) and $\hat{\sigma}_- = 1/2(\hat{\sigma}_{\mathrm{x}} - i\hat{\sigma}_{\mathrm{y}})$, with $\hat{\sigma}_{\mathrm{z}}$, $\hat{\sigma}_{\mathrm{x}}$ and $\hat{\sigma}_{\mathrm{y}}$ given by:

$$\hat{\sigma}_z = \begin{bmatrix} 1 & 0 \\ 0 & -1 \end{bmatrix}$$

$$\hat{\sigma}_+ = \begin{bmatrix} 0 & 1 \\ 0 & 0 \end{bmatrix}$$

$$\hat{\sigma}_- = \begin{bmatrix} 0 & 0 \\ 1 & 0 \end{bmatrix}$$

The Pauli matrices exert the following operations: $\hat{\sigma}_+\,|g\rangle = |e\rangle$, $\hat{\sigma}_-\,|e\rangle = |g\rangle$ and are therefore called the raising and lowering operators, moreover $\hat{\sigma}_z\,|e\rangle = |e\rangle$ and $\hat{\sigma}_z\,|g\rangle = -\,|g\rangle$.

The second term of equation (1.1) refers to the Hamiltonian of the electromagnetic field, given by:

$$H_{\mathrm{field}} = \hbar\omega_{\mathrm{c}}\hat{a}^\dagger\hat{a} + \hbar\eta(\hat{a}e^{i\omega_{\mathrm{p}}t} + \hat{a}^\dagger e^{-i\omega_{\mathrm{p}}t}), \tag{1.3}$$

where here we consider ω_{c} as the cavity resonance frequency and ω_{p} as the pump frequency driving the cavity at a rate η. The first term on equation (1.3) counts the number of photons in the cavity, the second one represents a classical pump field.

The interaction is given by

$$H_{\mathrm{interaction}} = -\hat{\mu}\cdot\hat{E}. \tag{1.4}$$

where $\hat{\mu}$ describes the dipole matrix operator and $\hat{E}$ the electromagnetic field. Both of these quantities are quantised and this term can be rewritten as:

$$H_{\mathrm{interaction}} = \hbar g(x)(\hat{a} - \hat{a}_-^\dagger)(\hat{\sigma}_- + \hat{\sigma}_+). \tag{1.5}$$

Upon expanding this expression we obtain four terms, two of which can be eliminated using the Rotating Wave Approximation (RWA), which discards terms oscillating at slower rate, to give:

$$H_{\mathrm{interaction}} = \hbar g(x)(\hat{\sigma}_+\hat{a} + \hat{\sigma}_-\hat{a}^\dagger). \tag{1.6}$$

Here the interaction strength is given by the coupling rate $g(x) = g_0 \cos(kx)$, which is position dependent. This rate can also be used to re-express the cooperativity as $C = \frac{g_0^2}{2\gamma\kappa}$, with κ and γ the atomic field and cavity field decay rates respectively. The strong-coupling regime in cavity QED corresponds to the condition $g_0 > \kappa, \gamma$.

At this point we would like to "ignore" the evolution of the free Hamiltonian, *i.e.* $H_{\text{atom}} + H_{\text{field}}$ and to only consider the evolution of the interaction Hamiltonian. To this aim we apply a unitary transformation which has the effect of putting us in a frame rotating with the free evolution of the oscillator, relative to this frame, we only see changes due to the interaction, and we eliminate the time dependence of the problem. After applying the unitary transformation given by $U = e^{i\omega_{\text{p}} t(\hat{\sigma}_z) + \hat{a}^\dagger \hat{a}}$, such that $\hat{a} = U^\dagger(t)\hat{a}U(t)$ and $\hat{\sigma}^- = U^\dagger(t)\hat{\sigma}^- U(t)$ and defining the detuning of pump, cavity field and atomic frequency as: $\Delta_{\text{c}} = \omega_{\text{p}} - \omega_{\text{c}}$ and $\Delta_{\text{a}} = \omega_{\text{p}} - \omega_{\text{a}}$ we obtain the following Hamiltonian:

$$H = \frac{p^2}{2m} + V_{\text{ext}}(x) - \hbar\Delta_{\text{a}}\hat{\sigma}_z - \hbar\Delta_{\text{c}}\hat{a}^\dagger\hat{a} + \hbar\eta(\hat{a} + \hat{a}^\dagger) + \hbar g(x)(\hat{\sigma}_+\hat{a} + \hat{\sigma}_-\hat{a}^\dagger) \quad (1.7)$$

This model can be generalised to an ensemble of atoms by summing over the contribution of each atom to the atomic Hamiltonian and the interaction Hamiltonian, in which case the model is known as the Tavis-Cummings model.

Now, when considering a Bose-Einstein condensate, we are interested in the coupling between the external degree of freedom and the cavity light field. We consider the BEC to be in its ground state, and the detuning Δ_{a} between the light resonance and the atomic resonance is large, *i.e.* we are in the "dispersive" regime. In this situation, the probability to excite an atom to the higher state is very small, therefore we can perform an adiabatic elimination of the excited state. This results in an effective Hamiltonian of the form:

$$H_{\text{eff}} = \frac{p^2}{2m} + V_{\text{ext}}(x) - \hbar\Delta_{\text{c}}\hat{a}^\dagger\hat{a} + \hbar\eta(\hat{a} + \hat{a}^\dagger) + \hbar\frac{g^2(x)}{\Delta_{\text{a}}}\hat{a}^\dagger\hat{a} \quad (1.8)$$

where the last term now can be interpreted as a shift of the cavity resonance due to the interaction between the atoms and the light.

In a many body formalism [25], the atomic field operators $\Psi(x)$ and $\Psi(x)^\dagger$ are

introduced, leading to:

$$H = \int dx \Psi(x)^\dagger \left(-\frac{\hbar^2}{2m}\nabla^2 + V_{\text{ext}}(x) + \hbar\frac{g^2(x)}{\Delta_\text{a}}\hat{a}^\dagger\hat{a} \right) \Psi(x) - \\ - \hbar\Delta_\text{c}\hat{a}^\dagger\hat{a} + \hbar\eta(\hat{a} + \hat{a}^\dagger) \tag{1.9}$$

the last term within the integral can be interpreted both as a dispersive shift of the cavity resonance due to the presence of the atoms, or a potential which shifts the position of the atoms. It expresses the backaction between light and atoms.

The description developed up to now is for a pump laser parallel to the cavity direction. For a standing wave pump which is transverse to the cavity instead of parallel, the situation varies and self organisation phenomena are observed, due to the interference effects between the pump light field and the cavity light field. In this scenario the pump photons impinge on the atoms which are excited and are able to radiate back into the cavity mode. The cavity mode hence becomes populated. In the dispersive limit (or large detuning limit), the single particle Hamiltonian in (1.6) can be recasted as:

$$H = \frac{p^2}{2m} + V_{\text{ext}}(x) - \hbar\Delta_\text{c}\hat{a}^\dagger\hat{a} + \hbar\eta(\hat{a} + \hat{a}^\dagger) + \frac{\hbar}{\Delta_\text{a}}(g(x)\hat{a}^\dagger + \Omega(z))(g(x)\hat{a} + \Omega(z)) \tag{1.10}$$

with $\Omega(z)$ being the coupling laser Rabi frequency which is space dependent: $\Omega(z) = \Omega\cos(kz)$ and transverse to the cavity coupling rate $g(x)$ defined as before as $g(x) = g_0\cos(kx)$. This corresponds to:

$$H = \frac{p^2}{2m} + V_{\text{ext}}(x) - \hbar\Delta_\text{c}\hat{a}^\dagger\hat{a} + \hbar\eta(\hat{a} + \hat{a}^\dagger) + \\ + \hbar\frac{g_0}{\Delta_\text{a}}\cos^2(kx)\hat{a}^\dagger\hat{a} + \hbar\frac{\Omega^2}{\Delta_\text{a}}\cos^2(kz) + \hbar\frac{g_0\Omega}{\Delta_a}\cos(kx)\cos(kz)(\hat{a} + \hat{a}^\dagger) \tag{1.11}$$

where the last three terms describe respectively the atom-cavity coupling, the static potential from the pump standing wave and a checkerboard lattice potential which depends on the atom position. Due to the interference of the two sinusoidals, photons from the pump can be scattered into the cavity only if the atoms are occupying a lattice with a λ periodicity, otherwise they experience destructive interference. Depending on the position of the scattering atoms, the phase of the scattered photons varies. Once photons are present in the cavity, they also strengthen the checkerboard potential. This marks the onset of a self-organised checkerboard lattice potential. However, if on one hand the scattering is only maintained for a

specific spatial organisation of the atoms, on the other hand the kinetic energy term is minimised for a homogeneous density distribution. The checkerboard potential and the kinetic energy terms battle in order to reach a stable situation. Therefore a threshold arises for the onset of the self organised phase. This has been shown to be a second order phase transition, with the relative phase between pump and cavity field and the number of atoms on either odd or even checkerboard sites as the parameters which display a broken symmetry [1].

1.1.3 The Cavity experiment

The cavity experiment in Tilman Esslinger's group at ETH is an experiment which involves a BEC loaded on a 3D optical lattice embedded in a high finesse optical cavity [23], [26], [1]. There are several similar experiments around the world with BEC in optical cavities, such as: [27], [28]. A schematic of the experiment is shown in Figure 1.2. In the experiment, a BEC of $\simeq 4 \times 10^4$ ^{87}Rb atoms trapped via an optical dipole trap in the center of a TEM_{00} mode of the cavity, is loaded onto a 2D lattice in the xz plane and split into a stack of 60 weakly coupled layers in the y direction. The lattices are respectively at a wavelength of λ_y = 670 nm and $\lambda_x = \lambda_z$ = 785.3 nm. The lattice beams create a lattice potential V_{2D} measured in

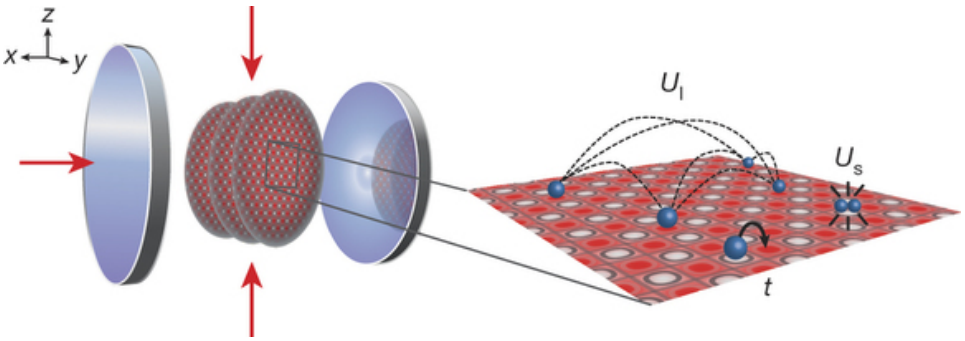

Figure 1.2: A BEC is loaded onto an optical lattice within an ultrahigh finesse cavity. Figure taken from [1].

units of the recoil energy E_{rec}. Moreover an overall harmonic potential results in a maximum density at the centre of the trap of 2.8 atoms per lattice site.

The beam along the z direction, as shown in Fig.1.2, pumps photons into the lattice. These photons scatter off the atoms into the cavity mode and mediate long range

interactions. There are two main scattering processes that occur in this system: a photon from the pump laser may be virtually absorbed by the condensate and scattered into the cavity mode, or a photon from the cavity mode may be scattered by the atoms into the pump standing wave field. This model, as discussed earlier, comprising a single atom (Jaynes-Cumming) or an ensemble of atoms (Tavis-Cumming) in a high finesse cavity, presents a quantum phase transition when the coupling term between the light and the atoms reaches a threshold value and self organisation takes over. The system of a trapped BEC in a cavity offers the possibility to realise the Dicke quantum phase transition where the self organisation in a checkerboard lattice corresponds to the Dicke transition [29].

When considering a single atom coupled to a single mode cavity in presence of a standing wave field, the Hamiltonian in the Rotating Wave Approximation (RWA) corresponds with equation 1.9 [29]. When moving to a description of the entire system instead of a single atom, a mean field approach is taken in which all atoms are occupying a single quantum state described by a wave function ψ normalized to the number of atoms [30]. A checkerboard lattice arises with geometry given by $\cos(kx)\cos(kz) = \pm 1$. The corresponding dynamic lattice potential is given by:

$$V(x,z) = V_0\cos^2(kz) + \hbar U_0|\alpha|^2\cos^2(kx) + \hbar\eta(\alpha+\alpha^*)\cos(kx)\cos(kz), \quad (1.12)$$

where the pump and atom resonance frequency detuning is more than five orders of magnitude and therefore only coherent scattering between pump and a single cavity mode is considered. Intracavity photons are created by Rayleigh scattering of laser photons into the cavity mode.

Light interference results in a strong depedence of the scattered intracavity field on the interatomic distance. For two atoms separated by odd integer multiples of the half-wavelength, the corresponding scattering amplitudes into the mode have the same magnitude but opposite sign, resulting in destructive interference and a vanishing cavity field amplitude. Atoms separated by even integer multiples of the half-wavelength, in contrast, have the field components scattered off the two atoms interfering constructively. The net result is the creation of a square-lattice potential that dynamically depends on the atomic position with periodicity $\frac{\lambda}{\sqrt{2}}$ in the diagonal direction of the $x-z$ plane, as shown in Figure 1.3. This is a a superlattice which distinguishes even from odd sites. The system is described by the usual

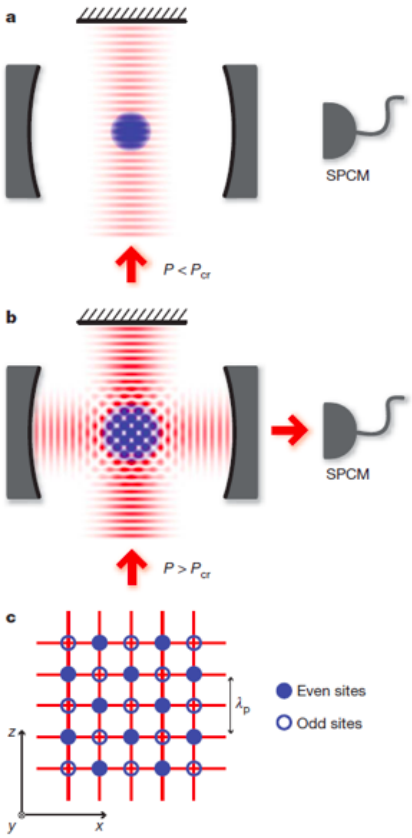

Figure 1.3: A checkerboard lattice arising from the scattering of pump photons into the cavity mode and viceversa. Figure taken from [29].

Bose-Hubbard Hamiltonian with the addition of a long range interaction term:

$$\hat{H} = -t \sum_{\langle e,o \rangle} (\hat{b_e}^\dagger \hat{b_o} + h.c.) + \sum_i \frac{1}{2} U_s \hat{n_i}(\hat{n_i} - 1) - \frac{U_l}{K} (\sum_e \hat{n}_e - \sum_o \hat{n}_o)^2 - \sum_{i \in e,o} \mu_i \hat{n_i}, \tag{1.13}$$

where the first term is the hopping term between nearest neighbours, e and o denote even and odd sites, with $\hat{b_i}$ the bosonic annihilation operator, $\hat{b_i}^\dagger$ the bosonic creation operator; the second term is the short range interaction term, with $\hat{n_i}$ the number operator; the third term describes the long range cavity mediated interactions and the last term the effective chemical potential in the Grand Canonical ensemble, h.c. denotes the hermitian conjugate.

This Hamiltonian is obtained by considering first a single particle Hamiltonian,

then moving to a many-body formalism with the introduction of the bosonic field operators Ψ and $\Psi^\dagger$ in second quantization and expanding the field operators in the basis of Wannier functions localised on different lattice sites [1].

The tuning parameters are the two interaction strengths: U_s and U_l. Both terms depends on the lattice potential V_{2D}, the long interaction strength is proportional to the lattice potential and inversely proportional to the detuning $\Delta_\mathrm{c} = \omega_z - \omega_\mathrm{c}$ with ω_c the cavity resonance frequency. Fine tuning the two parameters V_2D and Δ_c allows to enter a wide range of interaction strengths. The following section will explore in more detail the long range interaction term in the Hamiltonian. Later sections will also add details on each of the terms governing the behaviour of the system. Due to the interplay between the interactions which arise in this scenario,

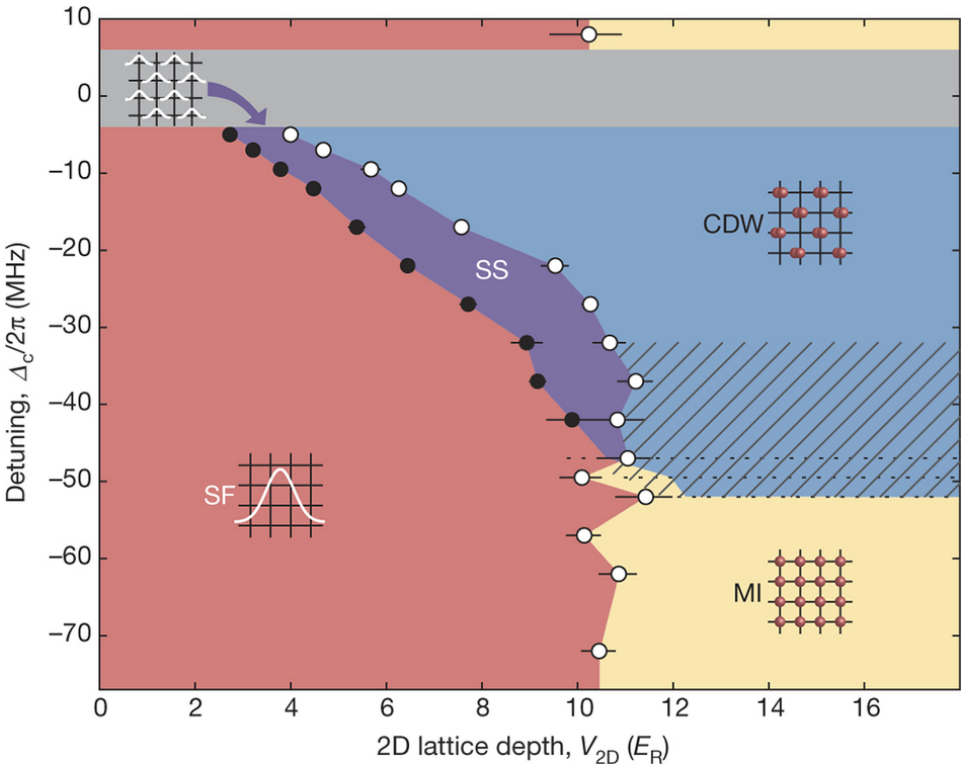

Figure 1.4: Quantum phase transitions which become accessible when cavity mediated long range interactions are active. Figure taken from [1].

three energy scales become accessible. The battle between competing energies results in an incredibly rich phase diagram as a function of the tuning parameters which displays four distinct phases: a superfluid (SF), a supersolid (SS), a Mott

insulator (MI) and a charge density wave (CDW). The phase diagram is shown in Figure 1.4 and shows the accessible experimental values for V_{2D} and Δ_c [31].

To summarise, a BEC cloud is trapped via an optical dipole trap in the center of the fundamental gaussian mode of the cavity. Then, it is split in 60 layers in the y direction by a standing wave, this forms layers in the $x - z$ plane which are then loaded onto 2D optical lattices formed by standing waves in the x and z directions. One of these two standing wave constitutes the free space lattice, the other is an intracavity lattice which is responsible for the scattering and delocalisation of photons in the cavity mode. The intracavity field mediates long range interactions, a type of interaction which had been seeked in the field of ultracold gases for a long time, but which seemed more challenging to achieve. The result of long range interactions in the Hamiltonian description of the system results in an additional term which turns out to be dependent on the density of atoms on the lattice sites. In particular the long range term depends on the difference on number of atoms on even and odd sites. The second chapter of this thesis will be particularly focused on studying the effect of this term on the dynamics of the BEC.

1.1.4 The IMPACT experiment

An additional level of complexity is achieved in the IMPACT experiment [3]. Here, two cavities are crossed at an angle of 60° with respect to a retro-reflected pump laser, as illustrated in the picture below. The BEC is located in the centre of the two cavities. The pump is retro-reflected by a mirror and thus forms a standing wave. The pump laser frequency is the same as the standing wave created within the two cavities, this frequency is far detuned from the atomic resonance frequency, stimulating coherent processes and scattering between photons and atoms and avoiding spontaneous emission to happen.

We can follow a photon from the pump to understand an example of a scattering process. The pump photon is scattered by an atom in the BEC into the mode of one of the two cavity fields. The atom experiences a recoil kick from the scattering in the opposite direction. Other processes include the scattering pump-atom-pump, cavity1-atom-cavity2 and viceversa, pump-atom-cavity and cavity1-cavity2. In reciprocal space, this produces a rich landscape of scattering events and wave vectors. We aim at understanding such scattering events and to be able to calculate the band structure for this rather complex system.

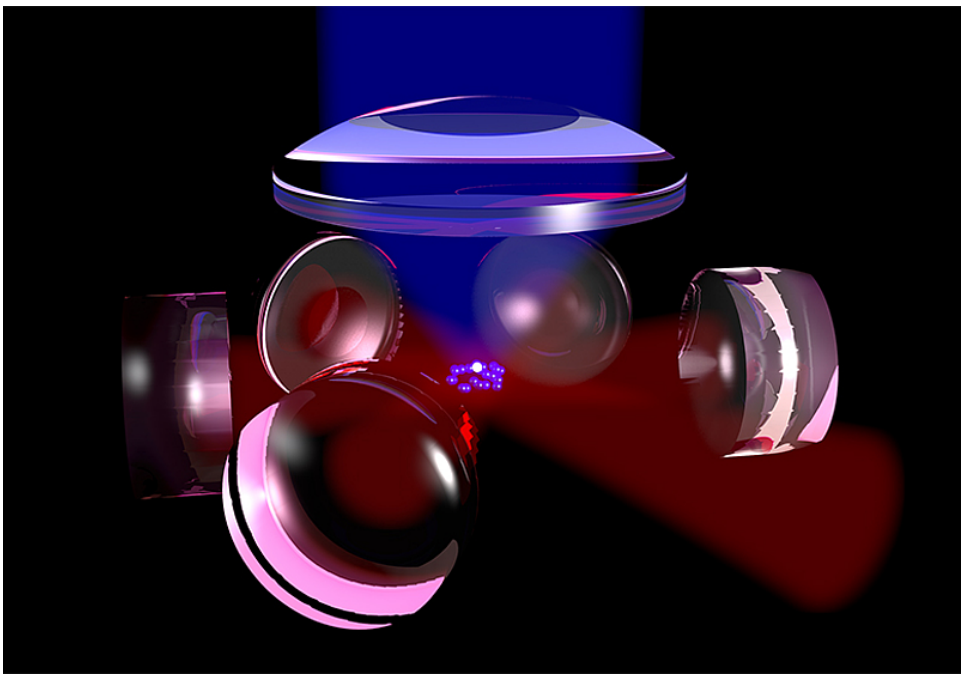

Figure 1.5: IMPACT experiment: a pump laser is retroreflected by a mirror and two crossed cavities are located at 60° angle to the pump. Figure taken from [1].

1.2 Objectives of the thesis

The following work is divided into two parts. The first chapter is focused on the study of collapse and revival dynamics of a BEC in presence of long range interactions. This work is based on the Cavity Experiment, it aims at understanding fundamental properties of Bose Einstein condensates when coupled to cavity fields. Based on our study, we propose a method to quantify the long range interaction strength in experiments involving this type of interactions. The work takes inspiration from Greiner's results from 2002 [2] on a very similar setup without the cavity and elaborates on it in order to understand the extended Hubbard Hamiltonian which results from the presence of the cavity. A toy model is developed and simulations are run on different types of situations mimicking the Cavity experiment.

The second part of the thesis tries to shed light on the theory behind the IMPACT experiment. Here the complex setup is studied in detail in order to identify all the possible scattering events and in order to determine the lattice structure in the

reciprocal space. A code is developed based on existing scripts for the Lattice experiment in Tilman Esslinger's group, in order to solve the Schroedinger's equation and compute the band structure for the system.

The simulations are written in Matlab for the first project and Python for the second project (due to adaptation of existing scripts). The main codes are included in the appendix. The appendix also contains a short account of an experimental project conducted in ICFO in the Quantum Photonics with Solids and Atoms group as a voluntary work, which was focused on the design, assembly and alignment of a high finesse cavity. We include this work in the appendix as the theoretical work performed over the master thesis revolves heavily around optical cavities.

Chapter 2

Collapse and revival dynamics in a BEC in presence of long range interactions

After your death, you will be what you were before your birth.

Arthur Schopenhauer

2.1 Collapse and revival dynamics

Collapses and revivals are fascinating and widespread wave phenomena. A collapse implies that an expectation value that initially has a high amplitude completely vanishes after a certain time, a revival that this pattern reaches again the original value.

In 1836, Henry Fox Talbot, one of the fathers of photography, discovered the fascinating phenomenon that was later named the Talbot effect [32]. What Talbot noticed was that holding a grating behind a lens illuminated by a light source would reproduce the grating pattern even when the grating was not at the focus of the lens. The puzzling effect did not raise much interest until Lord Rayleigh in 1881 formalised the effect and showed it could be a useful way of reproducing grating patterns. Later on the effect was again forgotten. In more recent years, parallel to the development of the quantum theory of light, it has become clear that the Talbot effect is a much richer and deeper phenomenon than Talbot himself expected. The

Talbot effect has roots in the extreme coherent interference of waves and in the fascinating limit between the quantum and the classical world.

Similarly to the Talbot effect, the Quantum carpet effect [33] shows the same "revival" of a quantum wavepacket representing an electron in an atom which propagates along the orbit of the electron. The wavepacket, described by a superposition of highly excited states, is originally localised on the electron's position. It is then left free to propagate and spreads along the orbit. However, after a specific time, the revival time, the wavepacket contracts again and recollects itself in its very same original form, producing a quantum revival. The origin of the Quantum carpet effect is, as for the Talbot effect, a result of coherent interference of waves. An other example of a quantum revival lies at the heart of the description of the interaction of light and matter: the Jaynes-Cummings (JC) model [34], which predicts oscillations of the atomic population of a two level system when irradiated by a single mode of the electromagnetic field.

In 2002, Markus Greiner and his collaborators asked themselves the following question: whether such collapse and revival dynamics could be observed in a BEC confined in an optical lattice. The question had been raised already by several theorists [35], [36], however no experimental realisation had been made. Greiner and his colleagues answered the question [2] by showing the presence of such dynamics in a BEC with short range interactions only.

Having at hand an experimental system as described in Chapter I, which allows us to add one ingredient: the cavity mediated long interactions, motivated us to ask once more the same question in this new scenario. The following chapter is organised as follows: first an overview of the work in search for collapse and revival dynamics is given, hence Greiner's findings are presented and our theoretical model proposed. Finally, we discuss the results obtained with our numerical simulations.

2.1.1 Collapse and revival in BEC

The phenomenon of collapse and revival dynamics in BEC has been gathering increasing interest over the years. The first authors to focus on the theoretical description of the BEC wave function were E. M. Wright and D. F. Walls [37] who, short after the BEC realisation by Ketterle [38], investigated the macroscopic wave

function for BEC in small atomic samples and its role as an order parameter. They found that the condensate wave function in small atomic samples exhibits collapse and revivals in time. At the same time, more efforts were put into understanding the fundamental features of the dynamics of the BEC by Lewenstein [35] and Imamoglu [36]. Collapse and revivals were studied in several different situations: for BEC in a double well potential, for untrapped BEC and for BEC confined in homogeneous potentials [39], [40], [41]; however, to our knowledge, there is no study of the phenomenon of collapse and revival of a BEC in a high finesse cavity.

2.2 Collapse and revival dynamics with short interactions only

One of the most fascinating aspects of a BEC is its similarity to a laser field. What makes the output light of a laser special is its coherence. Coherence is a property which quantifies the degree to which a wave in a specific point in space or time is related to the wave at the same location at a later time or at a different location at the same time. The coherent aspect of the light is mathematically expressed by having a fixed phase relationship between the waves considered. When waves interact with each other or with themselves, they interfere. Two waves with a constant phase difference between them are said to be perfectly coherent. It is precisely in this phase relationship that the similarity between a BEC and a coherent light field arises. Furthermore, the atoms in a BEC are all described by a unique macroscopic quantum wave function. In analogy with the photons in a laser, the atoms in a BEC all belong to the same spatial mode and have the same energy.

Despite the laser being the most 'classical' form of light and the BEC being the most 'classical' form of a matter wave, the BEC is composed by individual atoms which make its macroscopic matter field quantised. This granular property of the macroscopic wave function manifests itself when the dynamics of the system are considered. In the following, these dynamics will be discussed. The aim of this work is to understand fundamental aspects and behaviour of a BEC confined in a potential where long range interactions compete with short range interactions.

2.2.1 On site cold collisions

We begin by considering a BEC confined in a 3D optical lattice. The BEC is in all aspects a superfluid. In the superfluid regime where the lattice sites are fully separated, *i.e.* in the limit for which the tunnelling is suppressed (J=0), the macroscopic wavefunction occupies homogeneously the lattice sites. As the BEC is a collection of identical atoms, the most natural description of the system is to accomodate in each lattice site a superposition of Fock states (or number states). Moreover, since the lattice sites are all independent from one an other, the evolution of the system is simply determined by the short range interactions among atoms within the same potential well.

In analogy to the case discussed by Greiner [42], ultracold bosonic atoms interact via s-wave scattering, whereas inelastic three body collisions and higher partial wave scattering processes can be neglected for the parameters of the system. From scattering theory, we treat the problem of interactions between two ultracold bodies by using an ansatz which is made of an incoming plane wave and an outgoing spherical wave modulated by a scattering amplitude f:

$$\psi_k(\mathbf{r}) = e^{i\mathbf{k}\cdot\mathbf{r}} + f(\mathbf{k}, \frac{\mathbf{r}}{r}) \cdot \frac{e^{ikr}}{r}. \tag{2.1}$$

At low energies, the scattering amplitude can be approximated to a single number, the scattering length a, due to the fact that the angular properties of the scattering potential V cannot be resolved. The scattering length a is negative for effective attractive interactions and positive for effective repulsive interactions. In the case of Rb^{87}, a is positive.

The interaction potential between two neutral atoms is approximated by the Lennard-Jones potential:

$$V = \frac{A}{r^{12}} - \frac{B}{r^6}, \tag{2.2}$$

with r the interparticle distance, the first term describing the hard cores of the atoms and the second term the Van der Waals attraction.

However, in a many body system and additionally for a metastable BEC this scattering potential would lead to wrong thermodynamic results due to the presence of bound states, *i.e.* it would lead to a crystal rather than a dilute gas. For this reason

it is usual to substitute the full scattering potential with a pseudopotential which is able to reproduce the correct scattering length. The pseudopotential takes the form:

$$V(\mathbf{r}) = \frac{4\pi a\hbar^2}{m}\delta(\mathbf{r}), \tag{2.3}$$

where m is the mass of the particles. When two particles are placed in the ground state of a confining potential they collide. These collisions lead to an increase of the total energy by the interaction energy given by:

$$U(\mathbf{r}) = \frac{4\pi a\hbar^2}{m}\int d^3(\mathbf{x})|w(\mathbf{x})|^4, \tag{2.4}$$

with $w(\mathbf{x})$ the ground state wavefunction. This description is valid for a level spacing ω much larger than the total interaction energy. The cold collisions cause no dissipation but an increase in the total energy, as illustrated in the figure below.

When the situation is generalised to many atoms, each one of them interacts with the remaining $n-1$ and therefore the interaction Hamiltonian, after subraction of the ground state energy, is given by:

$$\hat{H} = \frac{1}{2}U\hat{n}(\hat{n}-1), \tag{2.5}$$

with $\hat{n}$ being the particle number operator given by $\hat{n} = \hat{a}^\dagger\hat{a}$ which counts the number of particles on the site .

This simple Hamiltonian provides the full description of the dynamics of the system for a single site. The collisions are coherent as the initial and final state are well defined. No energy is lost and the total energy increases by the interaction energy which depends non linearly on $\hat{n}$. This non linearity has an important effect on the dynamics of many body systems, as we will discuss shortly.

2.2.2 Ground state wavefunction

The interaction Hamiltonian described in the previous section has well known eigenmodes: Fock states. The corresponding eigenenergy is given by $E = \frac{U}{2}n(n-1)$ since $\hat{n}\,|n\rangle = n\,|n\rangle$. We also know that a superposition of Fock states is nothing but a Glauber or coherent state and that these states can be prepared in the laboratory.

Coherent states are indeed the quantum states of light which most closely resemble

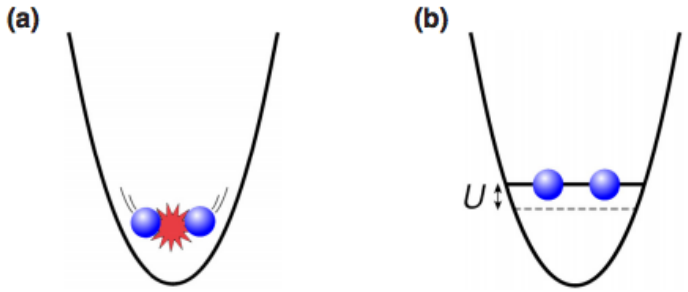

Figure 2.1: Collisions between atoms on the same lattice site, the total energy is increased by U. Figure taken from [2].

their classical limit, while preserving their quantum nature. "A Bose-Einstein condensate represents the most classical form of a matter wave, just as an optical laser emits the most classical form of an electromagnetic wave" [2]. Clearly our system belongs to the set of systems which present a strong classical limit, therefore it is reasonable to use a coherent state description for its ground state wavefunction. For a full derivation of Glauber states we refer to [43].

Coherent states have a series of interesting properties which make them useful. They are defined as the eigenstates of the annihilation operator:

$$\hat{a}\,|\alpha\rangle = \alpha\,|\alpha\rangle\,. \tag{2.6}$$

They can be written as a superposition of Fock states:

$$|\alpha\rangle = e^{-\frac{1}{2}|\alpha|^2} \sum_{n=o}^{\infty} \frac{\alpha^n}{\sqrt{n!}}\,|n\rangle\,, \tag{2.7}$$

where the Fock states are defined as:

$$|n\rangle = \frac{(a^\dagger)^n}{\sqrt{n!}}\,|0\rangle\,. \tag{2.8}$$

It follows by inserting the expression for the Fock states into the summation that the coherent states can be written also as a displaced vacuum state:

$$|\alpha\rangle = e^{-\frac{1}{2}|\alpha|^2+\alpha a^\dagger}\,|0\rangle = e^{\alpha a^\dagger - \alpha^* a}\,|0\rangle\,. \tag{2.9}$$

Coherent states are not orthogonal, the overlap between two coherent states is given by:

$$\langle\alpha|\,|\beta\rangle = e^{\frac{1}{2}|\alpha|^2-\frac{1}{2}|\beta|^2+\alpha^*\beta}; \tag{2.10}$$

the eigenvalue α is a complex number with argument and amplitude specified by:

$$\alpha = \sqrt{\bar{n}}e^{i\phi}, \tag{2.11}$$

where $\bar{n}$ is the average number of atoms and ϕ is the macroscopic field phase. The atom number distribution follows a Poissonian distribution for which the variance is equal to the mean, $\langle\bar{n}\rangle = \mathrm{Var}(n)$.

The ground state wavefunction for a single site system of BEC atoms in a confining potential can be prepared to be a coherent state. Such a state has a well defined phase and its eigenvalue α is a complex vector which describes a classical field Ψ. It is to note that one could also consider a different trial ground state wavefunction, which would not for example have problems with the truncation of the coherent state infinite sum. A trial wavefunction was considered and compared to the coherent state wavefunction, leading to very similar results. Next, we are interested in studying the time evolution of this ground state in presence of collisional interactions.

2.2.3 Time evolution with short range interactions

As the only interactions present in this model are the on site collisional interactions described earlier which occur between atoms on a specific site, we call this collisional interactions "short range" interactions. Later on we will expand our system to include the presence of "long range" interactions.

In order to understand how the system behaves, it is interesting to study its time evolution. The time evolution of a state is described by the time evolution operator $U(t)$ such that:

$$|\alpha(t)\rangle = U(t,0)\,|\alpha(0)\rangle \tag{2.12}$$

where $U(t) = e^{\frac{-iHt}{\hbar}}$ determines the evolution. For the Hamiltonian given before, it holds that $\hat{H}\,|n\rangle = E_n\,|n\rangle$, which means that the eigenstates of the Hamiltonian are number states with eingenenergy given by $E_n = \frac{1}{2}Un(n-1)$.

If we begin by considering a number state, than its time evolution is simply:

$$|n(t)\rangle = U(t,0)\,|n(0)\rangle = e^{\frac{-iHt}{\hbar}}\,|n(0)\rangle = e^{\frac{-iUn(n-1)t}{2\hbar}}\,|n(0)\rangle\,. \tag{2.13}$$

The number states acquire each a collisional phase which depends on the atom number. Each Fock state evolves differently depending on this phase. Moreover, the interaction energy is quadratic in the atom number. This nonlinearity is fundamental when one expands this treatment to coherent states. A coherent state is not an eigenstate of the Hamiltonian any longer. However, if one considers a coherent state with eigenenergies linear in n (for which $E_n \propto n$), for instance in the case of the harmonic oscillator, it is easy to see that a coherent state evolving in time will remain a coherent state up to a macroscopic phase factor:

$$|\alpha(t)\rangle = U(t,0)\,|\alpha(0)\rangle = \tag{2.14}$$

$$= e^{-\frac{1}{2}|\alpha(0)|^2} \sum_{n=0}^{\infty} \frac{(\alpha(0))^n}{\sqrt{n!}} e^{\frac{-i\omega\hbar(n+1/2)t}{\hbar}} \frac{(a^\dagger)^n}{\sqrt{n!}}\,|0\rangle\,. \tag{2.15}$$

Upon rearrangement this expression becomes:

$$|\alpha(t)\rangle = e^{-\frac{1}{2}|\alpha(0)|^2} e^{-\frac{i\omega t}{2}} \sum_{n=0}^{\infty} \frac{((\alpha(0))e^{-i\omega t}a^\dagger)^n}{n!}\,|0\rangle\,, \tag{2.16}$$

which is equivalent to:

$$|\alpha(t)\rangle = \exp(-\frac{1}{2}|\alpha(0)|^2 - \frac{i\omega t}{2} + \alpha(0)e^{-i\omega t}a^\dagger)\,|0\rangle\,, \tag{2.17}$$

this is nothing but a coherent state with a time dependent eigenvalue $\alpha(0)e^{-i\omega t}$ and a phase factor given by $e^{\frac{-i\omega t}{2}}$. For a Hamiltonian with linear eigenenergies, the coherent state remains a coherent state over time despite it not being an eigenstate of the Hamiltonian.

The situation is different when the Hamiltonian is non linear in the number state. In this case the coherent state evolves according to:

$$|\alpha(t)\rangle = e^{-\frac{1}{2}|\alpha(0)|^2} \sum_{n=0}^{\infty} \frac{(\alpha(0))^n}{\sqrt{n!}} e^{\frac{-iUn(n-1)t}{2\hbar}}\,|n\rangle\,, \tag{2.18}$$

which upon a similar rearrangement leads to:

$$|\alpha(t)\rangle = e^{-\frac{1}{2}|\alpha(0)|^2} \sum_{n=0}^{\infty} \frac{(\alpha(0)e^{iUt/2\hbar}a^\dagger)^n}{n!} e^{\frac{-iUn^2t}{2\hbar}},|0\rangle \tag{2.19}$$

the dependence on n^2 leaves an extra term which does not allow us to rewrite the expression as in (2.17).

Each number state acquires a different nonlinear collisional phase shift depending on its energy, which gives rise to an overall dephasing of the number states with respect to each other. This implies that the coherence, or the property to have a well defined phase, gets lost over time. However, due to the phase dependence, the coherence not only collapses but it also comes back after a defined time, as it will be discussed in the following section.

2.2.4 Collapse and revival

A BEC at $T = 0$ fully condensed is a collection of N atoms described all by the same single particle wave function. This is a many body system, and the many body wave function is given by a product over the single particle wave functions.

The BEC can be described also by an order parameter or macroscopic wave function. In an inhomogeneous system and for a non interacting BEC, this state corresponds to the ground state of the confining potential, for a periodic potential this state is a Bloch wave function with quasi momentum $\mathbf{q} = \mathbf{0}$. When considering a many body state as a superposition of states with different atom numbers and a well defined macroscopic phase, the order parameter can be defined as the expectation value of the single particle destruction operator:

$$\psi = \langle \hat{a} \rangle . \tag{2.20}$$

This quantity shows whether the many particle state can be described by a classical field ψ and it also is linked to the property of possessing a macroscopic phase. This field is given by:

$$\psi = \langle \alpha(t)| \, \hat{a} \, |\alpha(t)\rangle . \tag{2.21}$$

This quantity can be evaluated by inserting the expression for the time evolved coherent states and knowing that the Hamiltonian acts on the Fock state as:

$$\hat{H} \, |n\rangle = E_n \, |n\rangle = \frac{1}{2} U n(n-1) \, |n\rangle , \tag{2.22}$$

and the action of the annihilation operator on a number state:

$$\hat{a} \, |n\rangle = \sqrt{n} \, |n-1\rangle , \tag{2.23}$$

the resulting expression after algebraic manipulation reads:

$$\psi(t) = \sqrt{\bar{n}} \sum_n \frac{e^{-\bar{n}} \bar{n}^n}{n!} e^{i(E_n - E_{n-1})t/\hbar} = \sqrt{\bar{n}} \exp(\bar{n}(e^{\frac{-iUt}{\hbar}} - 1)), \tag{2.24}$$

which on a short timescale is approximated to:

$$\psi(t) \simeq \sqrt{\bar{n}} e^{\frac{-i\bar{n}Ut}{\hbar}} e^{\frac{-\bar{n}U^2t^2}{2\hbar^2}}. \tag{2.25}$$

The field is characterised by a revival and collapse dynamics with a characteristic collapse time $t_c = \frac{\hbar}{\sqrt{\bar{n}}U}$ and revival time $t_{\text{rev}} = \frac{h}{U}$, which are evident when recasting the above expression using the Euler's formula:

$$\psi(t) \simeq \sqrt{\bar{n}} e^{\frac{-\bar{n}U^2t^2}{2\hbar^2}} (\cos(\bar{n}(Ut/\hbar)) - i\sin(\bar{n}(Ut/\hbar))); \tag{2.26}$$

at the revival times, each number state acquires a phase which is given by $n \cdot 2\pi$: the state with $n = 1$ does not evolve, the state with $n = 2$ has accumulated a 2π shift, the one with $n = 3$ will have a phase of $3 \cdot 2\pi$, so all of the states have the same initial phase, modulo 2π. At t_{rev}, the many body macroscopic wavefunction is equivalent to the wavefunction at the initial time $t = 0$. The matter wave field entirely revives to its initial value. The revival and collapse dynamics is indeed a periodic oscillation with a period of t_{rev}. Below, the result obtained by Greiner for this model is shown for two revivals. [42]

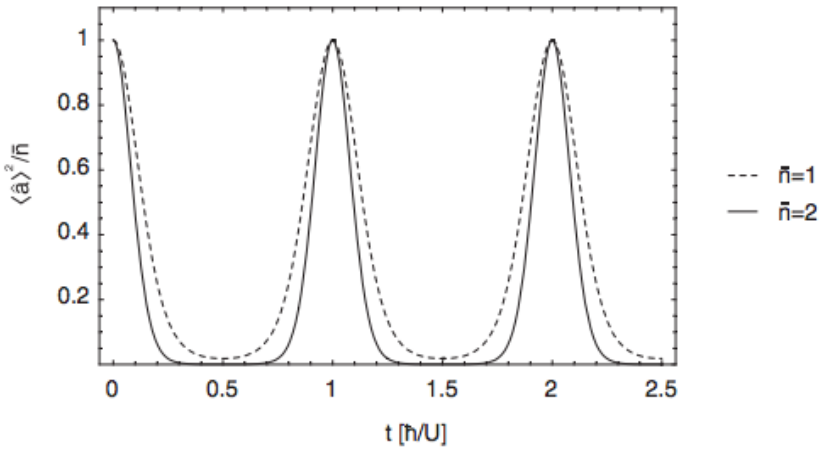

Figure 2.2: Periodic collapse and revival dynamics for $\bar{n} = 1$ and $\bar{n} = 2$. The matter wave field is plotted as $|\langle\hat{a}\rangle|^2$ vs time, periodic revivals are observed for $t_{rev} = h/U$. Note that the field revives completely to a value of 1. Figure taken from [42].

2.2.5 Experimental verification

A BEC of 2×10^5 ^{87}Rb atoms is loaded on a three dimensional optical lattice at a wavelength of $\lambda = 838$ nm [2]. At the centre of the lattice around 150000 sites are occupied with an average atom number per site up to 2.8. The atoms are trapped at the intensity maxima of the standing wave light field due to the dipolar force.

The main two results which confirm the presence of collapse and revival dynamics are shown below. In the former, the overlap between a stationary coherent state and a time evolving coherent state are shown. The phase is scrambled up to a time $\frac{t_{\text{rev}}}{2}$ (d), when despite $\psi = 0$ the system has evolved into an exact Schoedinger's cat state of two coherent state with a 180° phase difference. At the revival time (g), the initial coherent state is fully revived [2]. After preparing the BEC in a super-

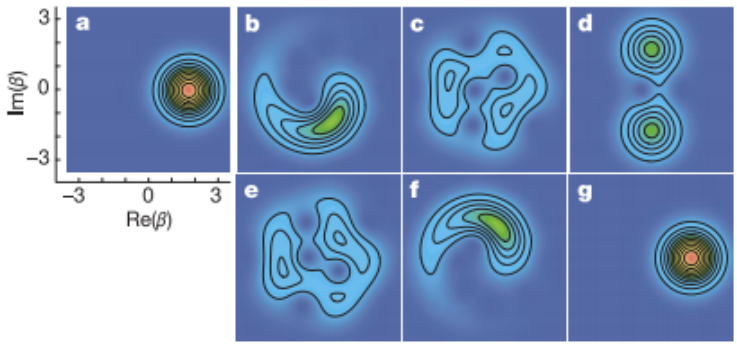

Figure 2.3: The overlap between an arbitrary coherent state and a dynamically evolved coherent state for an average number of atoms $\bar{n} = 3$ for different times. Figure taken from [2].

position of states, the experiment is performed by ramping up the lattice potential so that all the sites are independent and the tunnelling between sites is suppressed. The timescale for the jump in lattice potential is chosen carefully to be able to win any tunnelling effect while maintaining the state of the BEC in the ground state of the potential. Hence all the confining potentials are switched off at different hold times and the interference patter is observed, as shown in Figure 2.3.

The previous paragraphs have presented the system of a BEC in an optical lattice where the lattice potential was ramped up such that the sites became independent and the tunnelling was suppressed. The dynamics of this system were studied

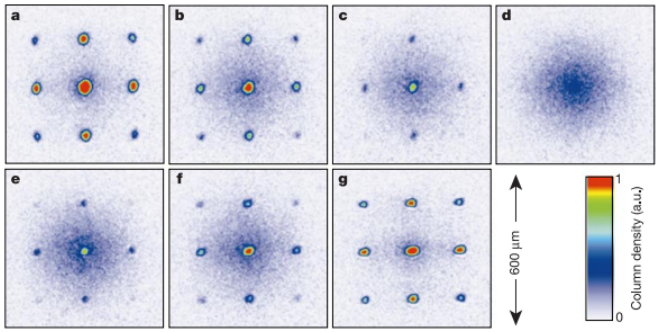

Figure 2.4: Absorption images after a time of flight period of 16 ms for different hold times t. The lattice potential is ramped from $V_A = 8E_r$ to $V_b = 22E_r$. The collapse is clearly visible at $t = 250$ µs and the revival for $t = 550$ µs. The collapse is due to a collapse of the matter wave field in each well. Figure taken from [2].

by modelling the ground state wave function as a superposition of number states evolving according to the interaction Hamiltonian alone. The theoretical analysis was carried out considering the evolution of the coherent state on a single lattice site. The dynamics of the system showed a collapse and revival behaviour. The theoretical predictions were then confirmed through experiments which showed the presence of a revival of the matter wave field of the whole system, owing to the phase relationships of the individual number states in each potential well.

In the following section we present an extension of this scenario, in which the same system is embedded in a ultra high finesse optical cavity. As shown in Chapter 1, the interaction between the cavity mode and the optical pump field leads the system to a Dicke regime whose net effect is to create a superlattice where even and odd sites become distinguishable. Due to the presence of the cavity, the Hamiltonian is extended to include an extra term which describes long range interactions. The next sections will present this new system in detail.

2.3 Collapse and revivals with long range interactions

The Cavity experiment in Tilman Esslinger's group motivates us to pose the question that Markus Greiner asked, for this new system. The main novel feature is the addition of a long range interaction term. This term, which has a quadratic dependence on the imbalance of atoms on even and odd sites, affects the dynamics

of the system. We are interested in understanding whether the collapse and revival dynamics persists in the presence of this long range interactions term and under which conditions. The following sections are organised as follows: first, the theoretical model is revisited to include the new term, hence our numerical model is described, followed by a discussion of the numerical results obtained.

2.3.1 Theoretical model

As discussed in the first chapter, the Hamiltonian for the cavity experiment is the Bose-Hubbard Hamiltonian with an additional term accounting for the effect of the cavity field. As this term depends on the global imbalance between even and odd sites, a description including a single site is not accurate anymore, and the model must take into consideration all the sites in the system. For our numerical simulation, we restrict to four lattice sites in order to capture the main features of the dynamics.

Expression (2.5) is expanded to:

$$\hat{H} = \sum_i \frac{1}{2} U_{\mathrm{s}} \hat{n}_i (\hat{n}_i - 1) - \frac{U_{\mathrm{l}}}{K} (\sum_e \hat{n}_e - \sum_o \hat{n}_o)^2, \tag{2.27}$$

where $\hat{n_i}$ counts the number of atoms on site i, U_{s} is the short range interaction potential, U_{l} is the long range interaction potential, K is the total number of sites and e and o denote the even and odd sites.

Again, we are interested in the dynamics of the system, in particular we are interested in the coherent properties of the system. In other words, we are asking whether a macroscopic phase is maintained during the time evolution and how it behaves. We expect the system to follow a similar evolution to the case presented in the previous chapter, where only the short interactions are present and the coherence gets lost after a characteristic time to then be revived again in a periodic fashion. The quantity of interest is again the order parameter, or matter wave field ψ given by:

$$\psi(t) = \langle \alpha(t) | \, \hat{a} \, | \alpha(t) \rangle \, , \tag{2.28}$$

where we now shift to the Heinsenberg picture, in which the time evolution is incorporated in the operators instead of in the states such that:

$$\psi(t) = \langle\alpha|\, \hat{a}(t)\, |\alpha\rangle\,. \tag{2.29}$$

This in turn is expanded to:

$$\psi(t) = \langle\alpha|\, e^{\frac{iHt}{\hbar}} \hat{a} e^{\frac{-iHt}{\hbar}}\, |\alpha\rangle\,, \tag{2.30}$$

with H given by equation (2.25) and the coherent states α defined as in (2.7). Due to the presence of the long range term, which includes double terms which connect different lattice sites, it is not possible to reduce this expression for H in order to obtain ψ such as in (2.23).

Note that the Hamiltonian contains only the number operators $\hat{n}_i$, $\hat{n}_e$, $\hat{n}_o$ and that the corresponding eigenstates are the Fock states. Here, we are evolving coherent states, a superposition of Fock states, which are all good eingenstates of the Hamiltonian, with the number of atoms in the sites as their eingenvalues. When considering more than one lattice site, the total ground state wavefunction is given by the tensorial product of the coherent states of each lattice site.

Both of the terms in the Hamiltonian are non-linear in the number operator, again this non linearity is at the core of the collapse and revival dynamics of the system. In the hope for the possibility of a mean field approach, we attempt to rewrite the long range interaction term of the Hamiltonian as a function of a single site number operator and an overall imbalance, however due to the quadratic form of the expression, it is not possible to rewrite the number states operators for the different sites. The interconnection between all sites, which produces a global interaction, remains present in the expression. As an example, consider a two sites system, this implies that the total coherent state is given by the tensorial product of the coherent state for each one of the sites:

$$|\alpha\rangle = |\alpha_1\rangle \otimes |\alpha_2\rangle\,, \tag{2.31}$$

where 1 and 2 denote the two sites. The time evolution will be given then by:

$$\psi(t) = \langle\alpha|\, e^{\frac{iHt}{\hbar}} \hat{a} e^{\frac{-iHt}{\hbar}}\, |\alpha\rangle = \langle\alpha_1| \otimes \langle\alpha_2|\, e^{\frac{iHt}{\hbar}} \hat{a} e^{\frac{-iHt}{\hbar}}\, |\alpha_1\rangle \otimes |\alpha_2\rangle\,, \tag{2.32}$$

with the Hamiltonian given by:

$$\hat{H} = \frac{1}{2} U_{\mathrm{s}} \hat{n}_1(\hat{n}_1 - 1) + \frac{1}{2} U_{\mathrm{s}} \hat{n}_2(\hat{n}_2 - 1) - \frac{U_{\mathrm{l}}}{K}(\hat{n}_2 - \hat{n}_1)^2. \tag{2.33}$$

When acting with the annihilation operator, one obtains a total of three terms in n_i which multiply three terms in $n_i - 1$, with U_s and U_l prefactors. This expression is much more complex than the simple, one factor expression in equation (2.24) due to the interconnectedness of different sites. As the number of sites increases, also the number of double terms increases.

In order to study the dynamics, we produce a Toy model for the system with which we run numerical simulations. The following section will describe the architecture of the model.

2.3.2 Numerical implementation

In order to produce numerical results, we implement a toy model for the system. We restrict to a number of four lattice sites, in order to capture the long range interactions effect.

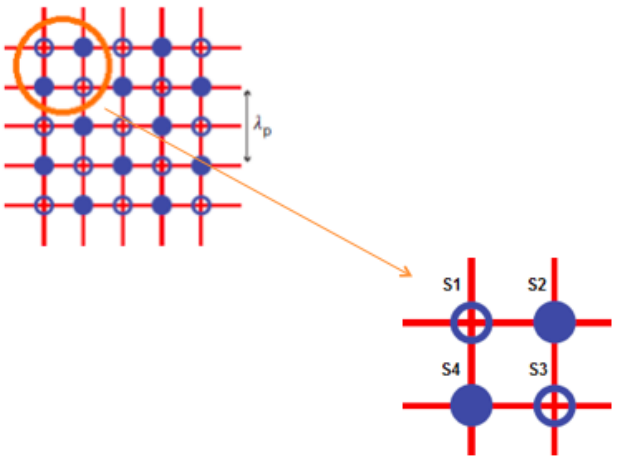

Figure 2.5: Toy model for a BEC in a high finesse optical cavity with even and odd sites, only four sites are considered.

We define the number operator on site i as:

$$\hat{n_i} = \begin{bmatrix} 0 & 0 & 0 \\ 0 & 1 & 0 \\ 0 & 0 & 2 \end{bmatrix}$$

and the annihilation operator given by:

$$\hat{a} = \begin{bmatrix} 0 & \sqrt{1} & 0 \\ 0 & 0 & \sqrt{2} \\ 0 & 0 & 0 \end{bmatrix}$$

The Hamiltonian acts on all the sites, therefore it has dimensions given by $(\#\mathrm{atoms})^{\#\mathrm{sites}}$: it is a matrix of dimensions 81×81. The sites can accommodate either none, one or two atoms, consistently with the quoted average number of atoms per site in the experiment given at the center of the lattice potential as up to 2.8. The coherent state α is then given by the first three terms in the Fock states sum, *i.e.* the infinite coherent state sum is truncated at the $n_{\max}$ chosen. This truncation has some consequences on the values up to which $|\langle a \rangle|^2$ revives as it will be discussed in the following section.

The full Hamiltonian for this toy model is given by:

$$\hat{H} = \hat{H}_{\mathrm{short}} + \hat{H}_{\mathrm{long}}, \tag{2.34}$$

with, for the four sites:

$$\hat{H}_{\mathrm{short}} = \frac{1}{2}U_{\mathrm{s}}\hat{n}_1(\hat{n}_1 - 1) + \frac{1}{2}U_{\mathrm{s}}\hat{n}_2(\hat{n}_2 - 1) + \frac{1}{2}U_{\mathrm{s}}\hat{n}_3(\hat{n}_3 - 1) + \frac{1}{2}U_{\mathrm{s}}\hat{n}_4(\hat{n}_4 - 1); \tag{2.35}$$

and denoting $\hat{n}_e = \hat{n}_2, \hat{n}_4$ and $\hat{n}_o = \hat{n}_1, \hat{n}_3$ the long range term is given by:

$$\hat{H}_{\mathrm{long}} = -\frac{U_{\mathrm{l}}}{K}((\hat{n}_2 + \hat{n}_4) - (\hat{n}_1 + \hat{n}_3))^2, \tag{2.36}$$

which is expanded to:

$$\begin{aligned} \hat{H}_{\mathrm{long}} = -\frac{U_{\mathrm{l}}}{K}((\hat{n}_1)^2 + (\hat{n}_2)^2 + (\hat{n}_3)^2 + (\hat{n}_4)^2 + \\ + 2\hat{n}_1\hat{n}_3 + 2\hat{n}_2\hat{n}_4 - \hat{n}_2\hat{n}_1 - \hat{n}_2\hat{n}_3 - \hat{n}_4\hat{n}_1 - \hat{n}_4\hat{n}_3). \end{aligned} \tag{2.37}$$

From this expression it is not immediately clear whether such a term could be recasted in a form which only has an overall imbalance term and the number operator for a single site.

We plot the result of the exact time evolution of the system as $|\psi|^2$ against time. The corresponding code is enclosed in the appendix. We expect to maintain the collapse and revival dynamics depending on the relative values of the interaction

strengths U_s and U_l. In the next section the main numerical results will be presented.

2.3.3 Numerical results

Throughout all the simulations the values for U_l and U_s need to be fixed. The experimental values are given in the plots and table below. Initially, three values for V_{2D} were selected in order to span the whole range: $V_{2D} = 5$, 10 and 15 E_{Rec}. These values corresponded with the values for U_s and U_l shown in Figure 2.8. Note that in order to estimate the long range interaction strength the number of sites K needs to be specified. In this case the experimental values are given for a system size of 10000 sites. This value is taken into account in the simulation, despite it being limited to 4 sites, the atoms on each site feel an interaction 'as if' the system size is effectively constituted by 10000 sites.

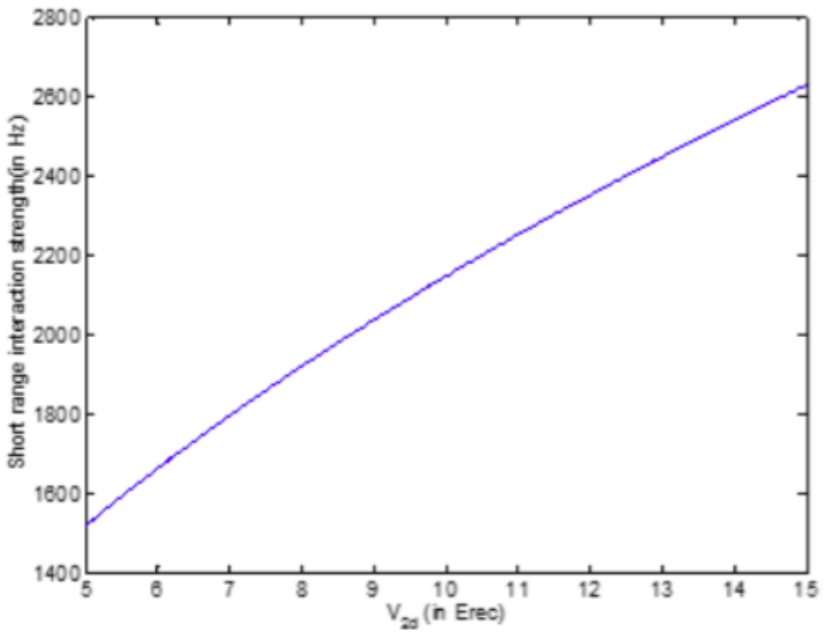

Figure 2.6: Short range interaction strength for $V_{670} = 25\ E_{rec}$. Data acquired from Tobias Donner.

The given values represent rough estimates for the interaction strengths. U_l and U_s display a dependence on the detuning Δ_c and the lattice potential V_{2D} given by [1]:

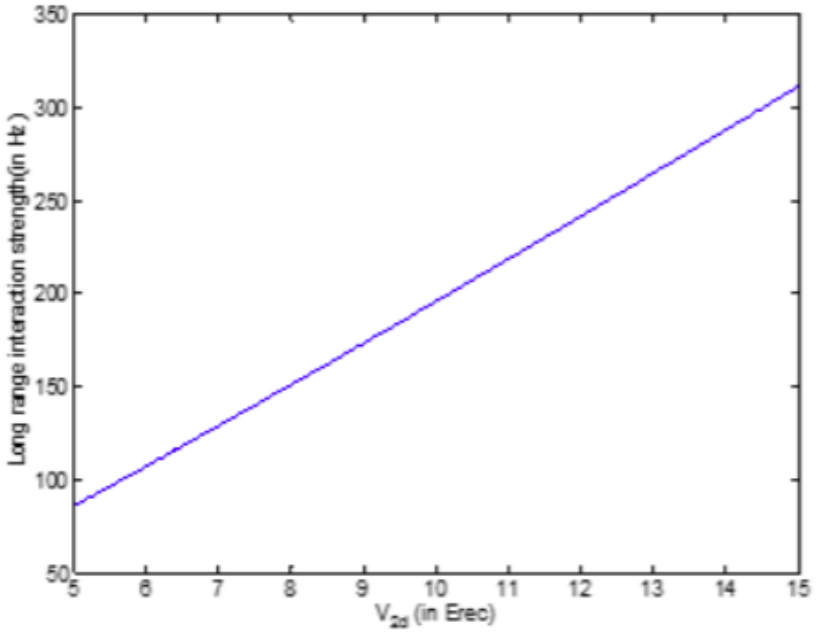

Figure 2.7: Long range interaction strength for V_{670} = 25 E_{Rec}, system size $K = 10000$ and detuning $\Delta_c = -30$ MHz. Data acquired from Tobias Donner.

$$U_l \propto \frac{V_{2\mathrm{D}}}{\Delta_c}. \tag{2.38}$$

These two quantities are the experimental parameters which are tuned in the laboratory, from them the interactions strengths are extracted. However in the laboratory sources of inhomogeneities are present, therefore these values serve as a guideline for realistic experimental values, but they need not to be considered with precision. Particularly, the value for U_{l} is to be regarded with care as it is just a rough estimate and it could be correct up to a factor of two.

This fact raises an interesting point: it is very difficult to precisely quantify the long range interaction strength of the system. Indeed, experiments on this system are rather focused on exploring different phases of matter in the presence of 'some' long range interactions. However, as it will be discussed shortly, the collapse and revival dynamics are very sensitive to the exact ratio of U_{s} and U_{l}, therefore the collapse and revival dynamics could be exploited as a method for providing a precise measurement of U_{l} in any similar setup. This proposal will be discussed in more detail in later sections.

V2D	5	10	15
UI (Hz)	80	190	310
Us (Hz)	1550	2150	2600

Figure 2.8: Experimental values for U_{s} and U_{l} as read from the provided plots at specific values of V_{2D} (in units of E_{Rec}).

To begin with, the collapse and revival dynamics as depicted in figure 2.2 are reproduced. The simulation is performed on a single site and with a $n_i = 0$, 1 or 2, for a $V_{\mathrm{2D}} = 10E_{\mathrm{Rec}}$ and $U_{\mathrm{s}} = 2150$ Hz. The time is given in units of $\frac{\hbar}{U}$, where we set $\hbar = 1$.
One feature of the result, which shows one of the limitations of the toy model, is the fact that the oscillations don't reach unity. We attribute this limitation to the truncation of the coherent state to a low number of Fock states. We check this hypothesis by simulating the dynamics for two, three, four and five atoms. The simulations show that the maximum value of $|a|^2$ increases when the number of particles in the system, and therefore the number of Fock states in the superposition, increases. However a higher number of particles significantly increases the computation time, while the collapse and revival dynamics remains unaltered. For this reason the simulations are performed for a maximum of two atoms per site.

The revival time $t_{\mathrm{rev}} = \frac{h}{U}$ is fully consistent with the numerical simulation. For $h = 1$, $U = 2150$ Hz and $t_{\mathrm{rev}} = \frac{h}{U} = \frac{1}{U} \simeq 0.00046s = 460\mu$s. The revival occurs in the simulation at $t(\frac{\hbar}{U}) = 0.00293$. Taking into account that $\hbar = \frac{h}{2\pi}$, we obtain $t_{\mathrm{rev}} = 0.00293/2\pi \simeq 0.00046$ s. Moreover this value is also similar to the experimental value quoted by Greiner [2] of 550 µs.

The system is then expanded to include the long range interactions. To being with, the coherent state is truncated to $n = 2$ and a $V_{\mathrm{2D}} = 5E_{\mathrm{Rec}}$ is chosen, corresponding to $U_{\mathrm{l}} = 1550$ Hz. By inspecting Fig 1.4 in Chapter 1, one can locate these values in the phase diagram. Several experimental values for the long interaction strength are chosen, however these values are a rough estimate as mentioned before.

The results show an interesting feature: collapses and revivals are clearly observed when the values of U_{s} and U_{l} are commensurate and their ratio is an integer. In the Hamiltonian, these two terms are in a linear superposition and the periodicity of the evolution is maintained when there is such a ratio between the two interaction strengths. The two interaction terms have opposite signs and are in competition. When the long interaction strength is much smaller then the short interaction strength, the dynamics is mainly determined by H_{short} and H_{long} acts as a perturbation. For the chosen value of U_{s}, plots for $U_{\mathrm{l}} = 90$ Hz and $U_{\mathrm{l}} = 155$ Hz are shown. The first one is in a non integer ratio with U_{s}, the second one is in an integer ratio.

As shown by figure 2.10 and 2.11, the commensurability of U_{s} and U_{l} is the factor which determines the presence or absence of periodic revivals. In particular in 2.11 well defined revivals are observed. The revival time t_{rev} is not anymore a trivial function of U_{s} only but it is determined by the dynamics of U_{l}. When trying to understand the revival time of the system, we first compute individually the dynamics in presence of either short or long range interaction for the same strength of U_{l} and U_{s}.

The result shows revival times at the same position, confirming that both interaction terms have the same $\frac{h}{U}$ dependence. However the shape of the curve is different, displaying a pure sinusoidal in the case of short range interactions and a more peaked oscillation in the case of long range interactions. We attribute this difference to the truncation of the coherent state wave function to two atoms. This truncation implies that, with short range interactions, only the term with $n = 2$ contributes in the superposition of Fock states and hence a pure sinusoidal is observed. With long range interactions, all of the Fock states contribute to the Hamiltonian, therefore higher frequencies are added which sharpen the sinusoidal into narrower peaks. The two curves are shown below. As expected, truncating the coherent state to n=3 makes the peaks narrower and increases their amplitudes.

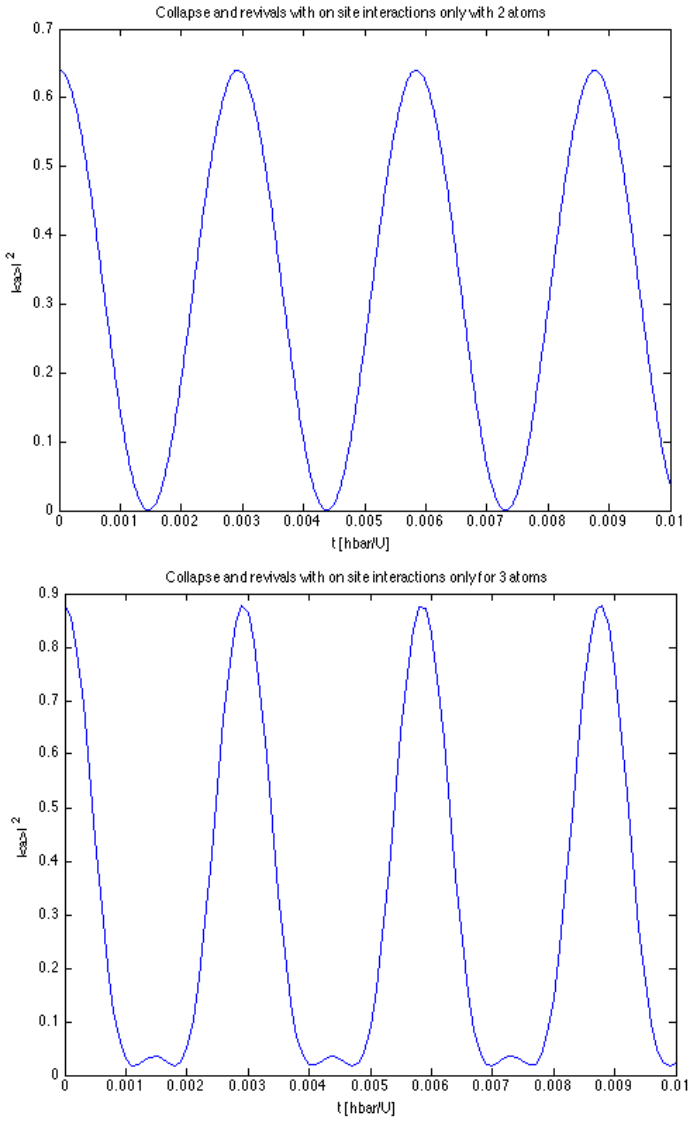

Figure 2.9: Collapse and revival dynamics for a single site with on site interactions only for U_{S}=2150 Hz for 2 and 3 atoms respectively. The effect of the truncation is evident.

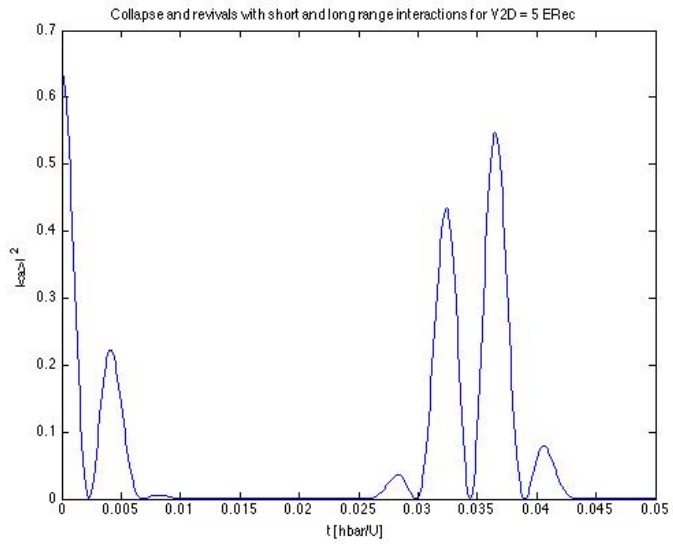

Figure 2.10: Collapse and revival dynamics with short and long interactions for $V_{2\mathrm{D}} = 5E_{\mathrm{Rec}}$ and $U_{\mathrm{l}} = 90$Hz, U_{s} and U_{l} are not commensurate.

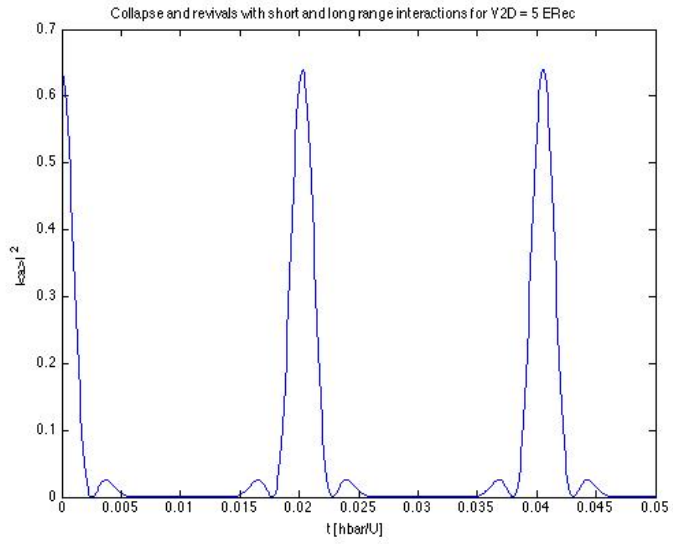

Figure 2.11: Collapse and revival dynamics with short and long interactions for $V_{2\mathrm{D}} = 5E_{\mathrm{Rec}}$ and $U_{\mathrm{l}} = 155$ Hz..

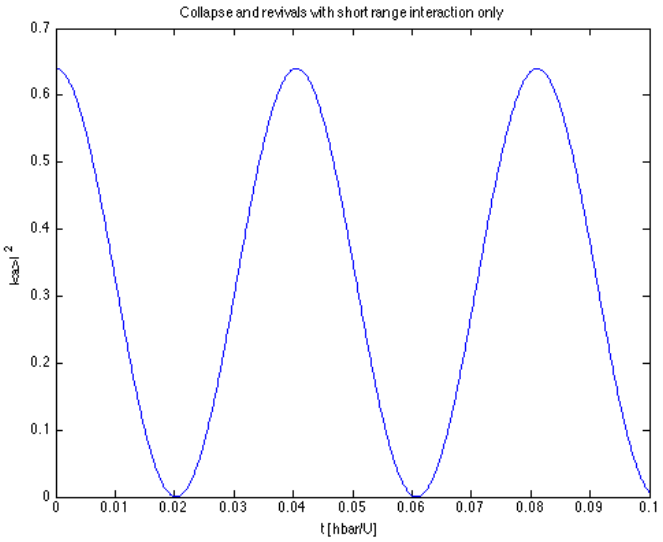

Figure 2.12: Collapse and revival with short interactions only for U_1=155 Hz.

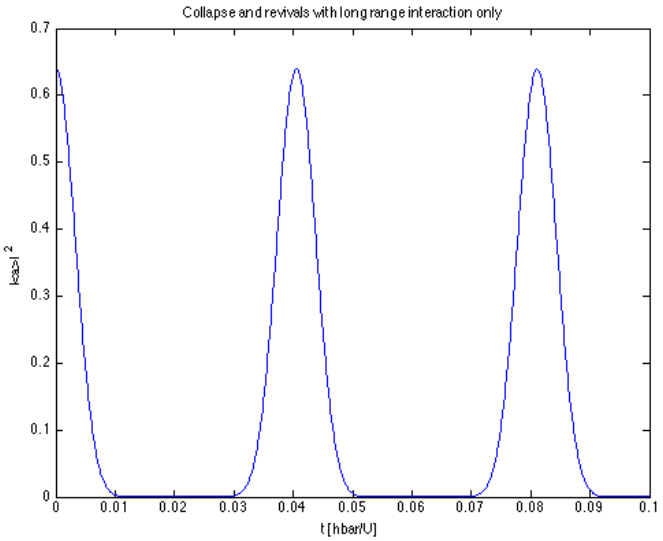

Figure 2.13: Collapse and revival with long interactions only for U_1=77.5 Hz.

In order to illustrate how the revival time changes when we have both a short and long term contribution we compute independently the dynamics in presence of either short or long range interactions alone, and overlay them. Figure 2.14 shows in blue the short range interactions acting alone and in red the long range interactions. It can be seen that the revivals happen at $t \simeq 0.008$ for the short range contribution and $t \simeq 0.04$ for the long range contribution.

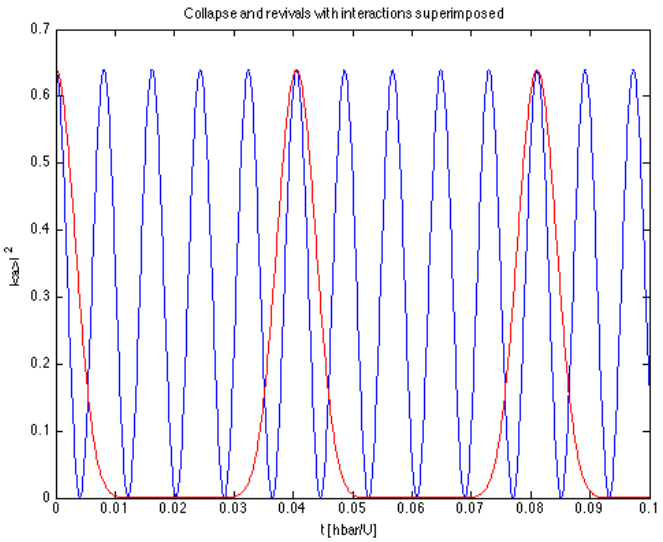

Figure 2.14: Short and long range contribution superimposed.

It does not come as a surprise to then have the dynamics shown in Fig 2.15 when both short and long interactions are active.

To study more in detail the dependence of revivals on the commensurability of the interaction strengths a commensurate ratio for U_s and U_l is chosen, specifically $U_\mathrm{l} = 77.5$ Hz and $U_\mathrm{s} = 1550$ Hz such that $\frac{U_\mathrm{s}}{U_\mathrm{l}} = 20$ and the value for U_l is swept around 77.5 Hz. Figure 2.16 nicely shows how a small 5 Hz variation is sufficient to loose the commensurability and therefore to loose the revivals. Among these peaks, it is easy to differenciate the value of 77.5 Hz (green curve) as it is the only one which fully revives at regular intervals. For this reason we propose to exploit the detection of the revivals in order to precisely determine the value for U_l. However it is to note that this method would be greatly dependent on the detection efficiency. Previous experiments with short range interactions showed that only up to a few revivals could be detected before the signal decayed due to noise and losses. It is an experimental challenge to be able to clearly identify a full revival

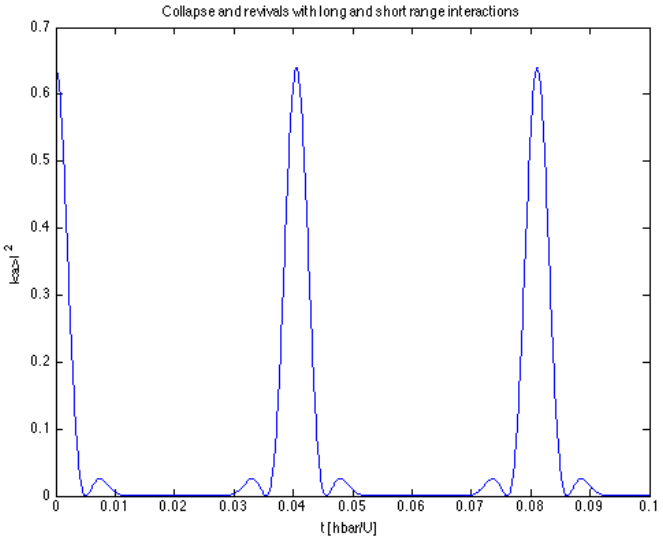

Figure 2.15: Short and long range contribution.

and to distinguish it from a simple 'peak', as it could be the case for the red and blue peaks close to t = 0.04 in Figure 2.16.

Finally, we include a plot of the full revivals occurring at specific commensurate ratios of U_{l} and U_{s}. Here the ratio between $|\langle\hat{a}\rangle|^2(t_{\mathrm{rev}})$ and $|\langle\hat{a}\rangle|^2(t_0)$, *i.e.* for the matter wave field at the revival time and at the initial time, is plotted as a function of the ratio between U_{s} and U_{l}. As Figure 2.13 shows, at integer values for the ratio of interaction strengths, the matter wave field is exactly the same at the revival time as at the initial time. This result reinforces the hypothesis that a full revival of the matter wave field occurs at the revival times for commensurate ratios of interaction strengths. Eventually this would be the result of a hypothetical experiment, in which one would observe full revivals only for exactly the commensurate values of the interaction strengths.

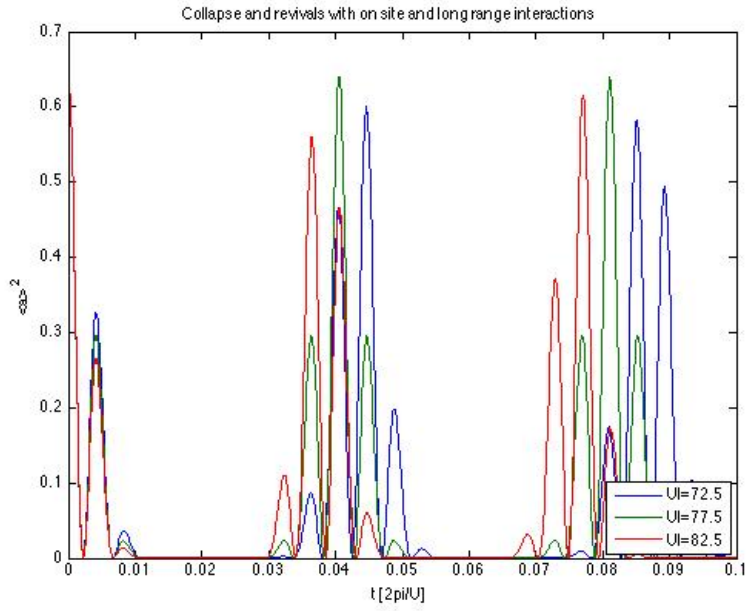

Figure 2.16: Sweeping U_{p} around the value 77.5 Hz.

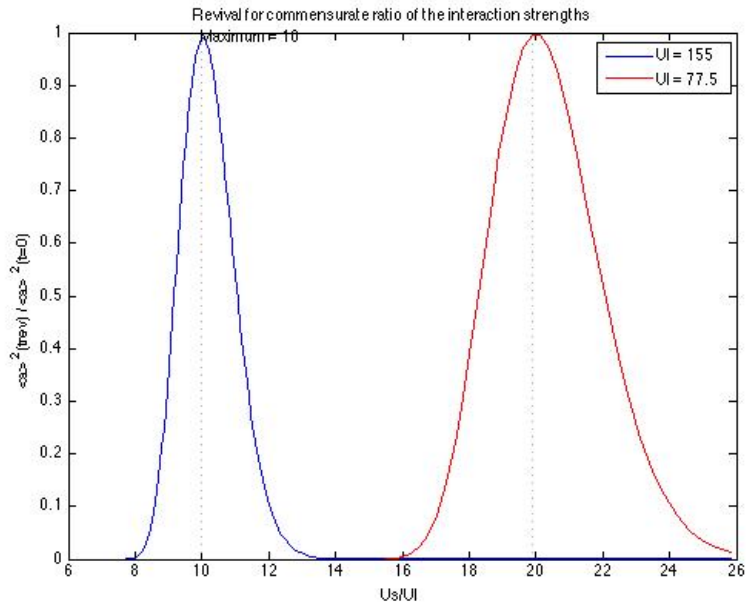

Figure 2.17: The full revival of the matter wave field at the revival times for specific commensurate values of the interaction strengths.

To summarise our story, motivated by the Cavity experiment in Tilman Esslinger's group at ETH, we have been interested in studying the collapse and revival dynamics of a BEC in an optical lattice within a high finesse cavity. We have begun our investigation by researching the phenomenon of collapse and revival and encountered it in the dynamics of BEC in optical lattices in presence of short range interactions. We have extended the study to include cavity-mediated long range interactions. Our simulations have shown that for commensurate values of the short and long interaction strengths collapse and revivals are preserved, but fragile. Moving away from a commensurate ratio of the two quantities produces an aperiodic decay of the matter wave field. Therefore the dynamics of the matter wave field could be used as a tool to precisely quantify the strength of the long range interactions present in the system. Our simulation correctly reproduces the dynamics for the system, however it is limited to 4 sites. An interesting development of the research would be to try to expand this system to one with a larger number of sites and particles, in order to assess the influence of the system size on the dynamics. An experimental verification would allow the study of fascinating collapse and revival phenomena.

During the master thesis months, several research outputs investigating the phenomenon of collapse and revival appeared in the field, see for instance: [44], [45] and [46], demonstrating the richness and fascination of the topic, and confirming that such a collapse and revival dynamics offers interesting and novel research avenues.

Chapter 3

Band structure calculations for the IMPACT experiment

We come spinning out of nothing,
scattering stars like dust!

Jalal ad-Din Muhammad Rumi

As described in the first chapter, the IMPACT experiment [3] is an evolution of the cavity experiment. Here the BEC is confined within two cavities at an angle with respect to the pump laser, as shown in Figure 3.1. The pump laser is also retroreflected via a mirror. Again, the pump laser frequency is far detuned with respect to the atomic frequency, therefore the photons from the pump are coherently scattered off the atoms into the two cavity or back into the pump field. As a result of the scattering process, the BEC Rubidium atoms receive a recoil kick which displaces them from their original position. By studying the allowed scattering processes we are interested in determining the distribution of atoms in the reciprocal space and then calculating the energy band structure of this system. Energy bands arise when considering a system which displays a periodicity in the potential. The Hamiltonian is exactly diagonalised to obtain the eigenenergies which correspond with the allowed energy values.

In the following sections, the theory of band structure is briefly presented, the cavity system is described and the optical potential is studied. Then the Hamiltonian term is implemented in order to calculate the band structure and the results obtained shown.

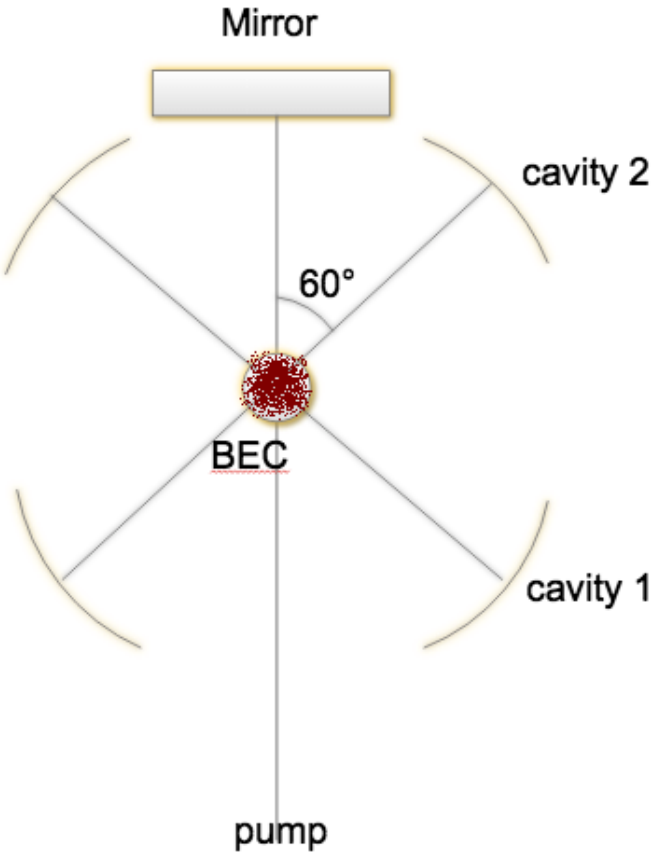

Figure 3.1: IMPACT experiment schematic diagram of the beams through the BEC.

3.1 Band Theory

Before presenting band theory, since we are interested in simulating a real condensed matter system by using a BEC in an optical potential, let us remind ourselves of some useful terminology of condensed matter physics [47], [48].

Condensed matter physics studies crystalline materials. A *crystal* is a repeating pattern of objects. A crystal is usually described by a *lattice* in combination with a *basis*. The lattice is an abstract infinite array of points in space which can be generated by a *translation vector*. A basis, on the other hand, is a collection of physical objects, for instance atoms or molecules. Convolving the lattice with the

basis results in the crystal. The arrangement of atoms looks the same at two points separated by a translation vector, and any property of the system, for instance a potential, will also exhibit the same periodicity. A *unit cell* is a region of space that, when repeated, fills all space. There is an infinite set of possible unit cell choices, the ones that have minimal volume are defined as *primitive unit cells*. A unit cell which is centred about a lattice point and hence reflects directly the symmetry of the lattice is called a *Wigner-Seitz cell*. This type of cell is obtained by starting from a lattice point and drawing vectors to any of the neighboring lattice points. Taking the perpendicular to the midpoint of these vectors gives planes, and the cell with the smallest volume about the origin bounded by these planes is the *Wigner-Seitz cell*. When including all types or translational invariance and invariance under other symmetry operations such as rotation, inversion and reflection, there are only 14 distinct types of lattices in 3 dimensions: they are the 14 *Bravais lattices*.

There are two main concepts in band theory. First, direct (or real) space and reciprocal space are related by a Fourier Transform. Secondly, the existence of band structure is a general consequence of the spatial periodicity of a lattice. Both of these concepts will be relevant in the next paragraph.

The concept of energy bands arises when considering the solutions of the Schroedinger's equation for a particle in a periodic potential. This is the case in any crystalline environment. The Schroedinger's equation with a potential takes the form:

$$H\psi = \left(\frac{-\hbar^2\nabla^2}{2m} + V(\mathbf{r})\right)\psi = E\psi, \tag{3.1}$$

where the potential $V(\mathbf{r})$ is periodic, *i.e.* $V(\mathbf{r}+\mathbf{T}) = V(\mathbf{r})$ and T is a lattice translational vector. Due to its periodic nature, the potential can be expressed as a Fourier series:

$$V(\mathbf{r}) = \sum_{\mathbf{G}} V_{\mathbf{G}} e^{i\mathbf{G}.\mathbf{r}}, \tag{3.2}$$

where $\mathbf{G}$ represents a vector in k-space (or reciprocal space). It can be shown from equation (3.2) that the existence of a lattice in real space implies the existence of a lattice in k-space. The vectors $\mathbf{G}$ define the reciprocal lattice. Due to the periodicity in the reciprocal space, the dispersion relation is not unique for each k but there is an infinite number of equivalent dispersion relations such that $E(\mathbf{k}) = E(\mathbf{k}+\mathbf{G})$. However, the periodicity results in having all the information enclosed in the prim-

itive unit cell of the reciprocal lattice, which is named the first Brillouin Zone (BZ).

In order to solve the Schroedinger's equation, we use an ansatz wavefunction as a sum of plane waves of the form:

$$\psi(\mathbf{r}) = \sum_{\mathbf{k}} C_{\mathbf{k}} e^{i\mathbf{k}.\mathbf{r}}. \tag{3.3}$$

Substituting the expressions for the wavefunction and the potential as a Fourier series in equation (3.2) leads to:

$$\sum_{\mathbf{k}} \frac{-\hbar^2 k^2}{2m} C_{\mathbf{k}} e^{i\mathbf{k}.\mathbf{r}} + (\sum_{\mathbf{G}} V_{\mathbf{G}} e^{i\mathbf{G}.\mathbf{r}})(\sum_{\mathbf{k}} C_{\mathbf{k}} e^{i\mathbf{k}.\mathbf{r}}) = E \sum_{\mathbf{k}} C_{\mathbf{k}} e^{i\mathbf{k}.\mathbf{r}}, \tag{3.4}$$

which after rearrangements becomes:

$$\sum_{\mathbf{k}} e^{i\mathbf{k}.\mathbf{r}} (\frac{-\hbar^2 k^2}{2m} - E) C_{\mathbf{k}} + \sum_{\mathbf{G}} V_{\mathbf{G}} C_{\mathbf{k}-\mathbf{G}} = 0. \tag{3.5}$$

Due to Born-von Karman boundary conditions [47], the coefficients of each term in the sum must vanish. Moreover one can consider solutions belonging only to the first BZ, rewriting $\mathbf{k} = \mathbf{q} - \mathbf{G}'$ (where $\mathbf{q}$ is a vector lying in the first BZ). One can also apply the change of variables $G \rightarrow G'' - G'$ and obtain:

$$(\frac{-\hbar^2 (\mathbf{q} - \mathbf{G}')^2}{2m} - E) C_{\mathbf{q}-\mathbf{G}'} + \sum_{\mathbf{G}''} V_{\mathbf{G}''-\mathbf{G}'} C_{\mathbf{q}-\mathbf{G}''} = 0, \tag{3.6}$$

where the coefficients $C_{\mathbf{k}}$ specify the form that the wavefunction ψ takes. For each vector $\mathbf{q}$ within the first BZ, there is a wavefunction $\psi_q(\mathbf{r}) = \sum_{\mathbf{G}} C_{\mathbf{q}-\mathbf{G}} e^{i(\mathbf{q}-\mathbf{G}).\mathbf{r}}$, which can be rewritten as:

$$\psi_q(\mathbf{r}) = e^{i\mathbf{q}.\mathbf{r}} \sum_{\mathbf{G}} C_{\mathbf{q}-\mathbf{G}} e^{-i\mathbf{G}.\mathbf{r}} = e^{i\mathbf{q}.\mathbf{r}} u_{j,\mathbf{q}}. \tag{3.7}$$

This means that the wavefunction is given by a plane wave with a wave vector within the first BZ and a function which has the same periodicity of the lattice. In other words, the eigenstates are made up by a sum of plane wave states which differ by a reciprocal lattice vector.

This demonstrates the Bloch's theorem, which states that the eingenstates ψ of a one-electron Hamiltonian can be chosen to be a plane wave times a function which has the same periodicity of the Bravais lattice. Each set of functions $u_{j,\mathbf{q}}$ results in a set of states with specific dispersion relations. The number of possible

wavefunctions in each band will be given by the number of distinct $\mathbf{q}s$ in the first BZ.

Bloch's theorem presents two limiting cases: a very weak potential (Nearly Free Electron model) and a very strong potential (Tight Binding model) [49]. Both models give rise to band structures and band gaps. In particular, within the Nearly Free Electron model, the potential is treated as a weak perturbation. A plane wave state characterised by a crystal momentum k can only scatter into a different state k' if the two are separated by a reciprocal lattice vector. Perturbation theory is then applied in order to calculate the dispersion relation $E(k)$. The presence of the weak potential results in a gap separating different bands at the position of the BZ boundary. Moreover, at the BZ boundary, the bands have a quadratic dispersion which can also be described by an effective mass. The following section will present the main ingredients for the calculation of the bands: the Hamiltonian and the optical potential for the system.

3.2 Hamiltonian and optical potential

In order to calculate the band structure, we first need to define a basis and a Hamiltonian for our system. For our geometry, where the two cavities are at a 60 $^\circ$ angle to the pump laser, we choose as our reciprocal lattice vectors:

$$\begin{aligned} \mathbf{k_p} &= k\hat{\mathbf{e}}_\mathbf{y}; \\ \mathbf{k_1} &= -k\sin\theta\hat{\mathbf{e}}_\mathbf{x} + k\cos\theta\hat{\mathbf{e}}_\mathbf{y}; \\ \mathbf{k_2} &= k\sin\theta\hat{\mathbf{e}}_\mathbf{x} + k\cos\theta\hat{\mathbf{e}}_\mathbf{y}, \end{aligned} \tag{3.8}$$

which for $\theta = \pi/3$ become:

$$\begin{aligned} \mathbf{k_p} &= k\hat{\mathbf{e}}_\mathbf{y}; \\ \mathbf{k_1} &= -k\frac{\sqrt{3}}{2}\hat{\mathbf{e}}_\mathbf{x} + k\frac{1}{2}\hat{\mathbf{e}}_\mathbf{y}; \\ \mathbf{k_2} &= k\frac{\sqrt{3}}{2}\hat{\mathbf{e}}_\mathbf{x} + k\frac{1}{2}\hat{\mathbf{e}}_\mathbf{x}, \end{aligned} \tag{3.9}$$

where $\mathbf{k_p}$ is the wavevector for the pump laser, $\mathbf{k_1}$ for the first cavity and $\mathbf{k_2}$ for the second cavity. We notice that these three wavevectors are linked by the relation:

$$\mathbf{k_p} - \mathbf{k_1} = \mathbf{k_2}. \tag{3.10}$$

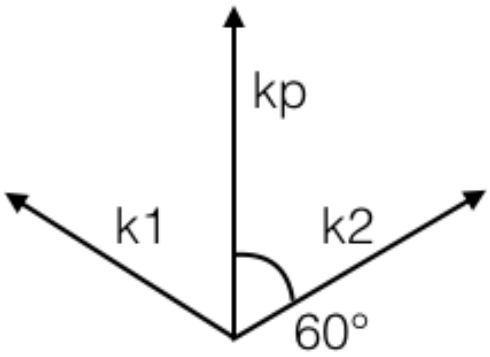

Figure 3.2: Reciprocal lattice vectors for the double cavity and pump setup.

This will be useful later as it will allow us to rewrite the reciprocal lattice vectors in terms of a new basis formed by $\mathbf{k_p}$ and $\mathbf{k_1}$.

The full Hamiltonian for the system [3] is given by:

$$\begin{aligned}\hat{H} =& -\hbar\Delta_1(\hat{a}_1^\dagger\hat{a}_1) - \hbar\Delta_2(\hat{a}_2^\dagger\hat{a}_2) + \iint_A \Psi^\dagger(x,y)[\frac{p_x^2+p_y^2+2p_x.p_y}{2m} \\ & \hbar\eta_1(\hat{a}_1^\dagger+\hat{a}_1)\cos(\mathbf{k_p}\cdot\mathbf{r}+\phi)\cos(\mathbf{k_1}\cdot\mathbf{r}) \\ & +\hbar\eta_2(\hat{a}_2^\dagger+\hat{a}_2)\cos(\mathbf{k_p}\cdot\mathbf{r}+\phi)\cos(\mathbf{k_2}\cdot\mathbf{r}) \\ & +\hbar\eta_3(\hat{a}_1^\dagger\hat{a}_2+\hat{a}_2^\dagger\hat{a}_1)\cos(\mathbf{k_1}\cdot\mathbf{r})\cos(\mathbf{k_2}\cdot\mathbf{r}) \\ & +\hbar U_\mathrm{p}\cos^2(\mathbf{k_p}\cdot\mathbf{r}+\phi)+\hbar U_1\cos^2(\mathbf{k_1}\cdot\mathbf{r}+\phi)\hat{a}_1^\dagger\hat{a}_1 \\ & +\hbar U_2\cos^2(\mathbf{k_2}\cdot\mathbf{r}+\phi)\hat{a}_2^\dagger\hat{a}_2]\Psi(x,y)dxdy.\end{aligned} \tag{3.11}$$

Here, Δ represents the detuning of the pump with respect to the resonance frequency: $\Delta_i = \omega_\mathrm{p} - \omega_i$, $\eta_i = \frac{\Omega_\mathrm{p} g_\mathrm{i}}{\Delta_A}$, with $i = 1, 2$ for cavity 1 and cavity 2 respectively, $\eta_3 = \frac{g_1 g_2}{\Delta_A}$, $U_\mathrm{p} = \frac{\Omega_\mathrm{p}^2}{\Delta_A}$ and $U_\mathrm{i} = \frac{g_\mathrm{i}^2}{\Delta_A}$, for $i = 1, 2$. The values for the tunable parameters g_i, Δ_A and Ω_p will be discussed shortly.

The first two terms represent the energy of the photons in the cavity fields, with the annihilation and creation operators for photons represented as usual by $\hat{a}$ and $\hat{a}^\dagger$, the terms within the integral represent the interaction terms between the light

and the BEC atoms, with Ψ and $\Psi^\dagger$ being the atomic field operators which create and annihilate particles. The integration is carried over the Wigner-Seitz cell A. The transverse pump at λ_p is far detuned from the atomic transition but closely detuned from the cavity resonances, thus suppressing absorption but allowing off-resonant Raman processes.

Within the integral we identify the kinetic term, given by $p^2/2m$, and the optical potential term, given by:

$$\begin{aligned}\hat{V}(\mathbf{r}) =&\hbar\eta_1(\hat{a}_1^\dagger+\hat{a}_1)\cos(\mathbf{k_p}\cdot\mathbf{r}+\phi)\cos(\mathbf{k_1}\cdot\mathbf{r})\\ &+\hbar\eta_2(\hat{a}_2^\dagger+\hat{a}_2)\cos(\mathbf{k_p}\cdot\mathbf{r}+\phi)\cos(\mathbf{k_2}\cdot\mathbf{r})\\ &+\hbar\eta_3(\hat{a}_1^\dagger\hat{a}_2+\hat{a}_2^\dagger\hat{a}_1)\cos(\mathbf{k_1}\cdot\mathbf{r})\cos(\mathbf{k_2}\cdot\mathbf{r})\\ &+\hbar U_\mathrm{p}\cos^2(\mathbf{k_p}\cdot\mathbf{r}+\phi)+\hbar U_1\cos^2(\mathbf{k_1}\cdot\mathbf{r}+\phi)\hat{a}_1^\dagger\hat{a}_1\\ &+\hbar U_2\cos^2(\mathbf{k_2}\cdot\mathbf{r}+\phi)\hat{a}_2^\dagger\hat{a}_2.\end{aligned} \tag{3.12}$$

This potential term contains all the possible interactions between the light and the atoms. The photons are scattered by the BEC atoms into the different light fields. The pump light is described by a standing wave.

If we focus on this potential, we can identify the first term as the interaction term between the pump and the first cavity, the second as the interaction between the pump and the second cavity, the third term as the cavity 1 to cavity 2 interaction, the fourth term arising from photons which come from the pump and are scattered off by the atoms back into the pump, the fifth as photons from the first cavity being scattered back into the same cavity and the last one photons from the second cavity being scattered back into the same cavity. The last three terms represent lattice potentials for the transverse pump and the two cavities respectively.

In order to visualise more clearly the scattering events, it is helpful to rewrite the sinusoids as exponentials. We consider the first term in the potential as an example:

$$\begin{aligned}\hat{V}(\mathbf{r}) =&\hbar\eta_1(\hat{a}_1^\dagger+\hat{a}_1)\cos(\mathbf{k_p}\cdot\mathbf{r}+\phi)\cos(\mathbf{k_1}\cdot\mathbf{r}) =\\ &\hbar\eta_1(\hat{a}_1^\dagger+\hat{a}_1)[e^{i\phi}(e^{i(\mathbf{k_p}\cdot\mathbf{r}+\mathbf{k_1}\cdot\mathbf{r})}+e^{i(\mathbf{k_p}\cdot\mathbf{r}-\mathbf{k_1}\cdot\mathbf{r})})\\ &+e^{-i\phi}(e^{i(-\mathbf{k_p}\cdot\mathbf{r}+\mathbf{k_1}\cdot\mathbf{r})}+e^{i(-\mathbf{k_p}\cdot\mathbf{r}-\mathbf{k_1}\cdot\mathbf{r})})],\end{aligned} \tag{3.13}$$

which corresponds with the scattering events illustrated in Figure 3.3. Note that ϕ represents the pump laser phase (varying from 0 to $\pi/2$), which is implemented by displacing the retroreflectingretroreflecting mirror, and is crucial in defining the

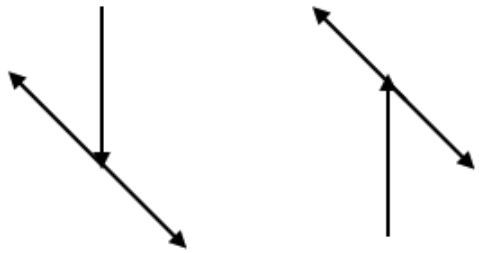

Figure 3.3: Scattering events from the pump into cavity 1.

geometry of the optical lattice.

It is possible to decompose each term in the potential in the same way to identify all of the possible scattering events which are depicted in Figure 3.4, yellow represents the pump-cavity scatterings, green the cavity$_i$-cavity$_j$ scattering, red the pump to pump scattering and blue the cavity$_i$ to cavity$_i$ scatterings. It is important to know all the allowed scattering events as these terms are present in the Hamiltonian which will be diagonalised to calculate the band structure.

The tunable quantities in the lab are the cavity couplings, the pump frequency and the pump-cavity detuning. These values correspond to: g_1 = g_2 = 2 $\pi\times$1.8 MHz for the cavity coupling rates, Δ_{A} = 2$\pi\times$ 2 THz for the pump-atom detuning and Ω_{p}=2$\pi\times$100 MHz for the pump Rabi frequency. We treat the creation and annihilation operators for the light fields as their coherent state amplitudes, where a coherent state is defined as $\alpha = |\alpha|e^{i\theta}$. These have a value of $|\alpha_1|$=$|\alpha_2|$=10. In the following, we always consider only the real amplitudes for the coherent states.

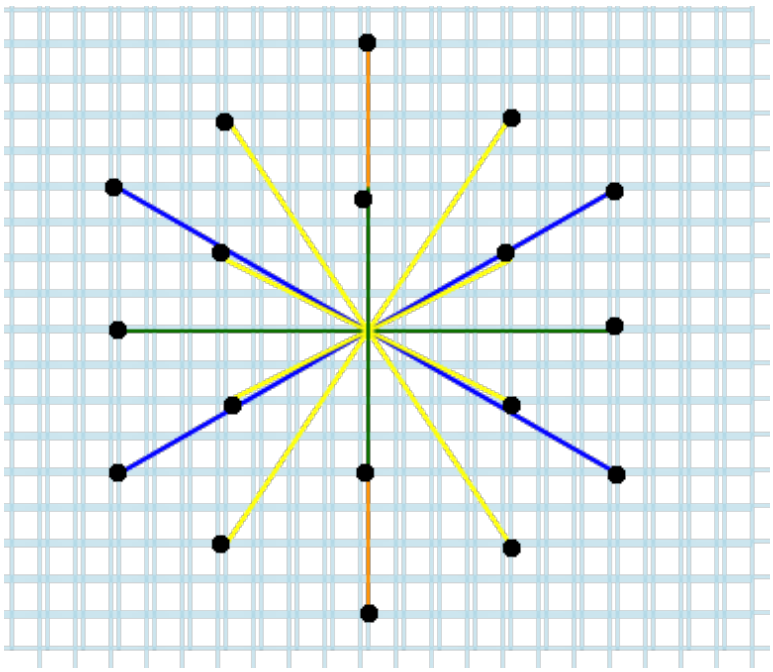

Figure 3.4: All the scattering processes between pump, atoms and cavities. Yellow lines represent the cavity-pump scatterings, orange the pump-pump scatterings, blue the cavity-other cavity scatterings and green the cavity-same cavity scatterings.

In the Hamiltonian, the coefficients for the terms correspond to:

$$\begin{aligned}
\eta_1 &= \frac{\Omega_{\mathrm{p}} g_1}{\Delta_{\mathrm{A}}};\\
\eta_2 &= \frac{\Omega_{\mathrm{p}} g_2}{\Delta_{\mathrm{A}}};\\
\eta_3 &= \frac{g_1 g_2}{\Delta_A};\\
U_{\mathrm{p}} &= \frac{\Omega_{\mathrm{p}}^2}{\Delta_A};\\
U_1 &= \frac{g_1^2}{\Delta_A};\\
U_2 &= \frac{g_2^2}{\Delta_A}.
\end{aligned} \tag{3.14}$$

Moreover we define the coefficients $A_1 = \hbar\eta_1(|\alpha_1|+|\alpha_1|)$, $A_2 = \hbar\eta_2(|\alpha_2|+|\alpha_2|)$, $A_3 = \hbar\eta_3(|\alpha_1||\alpha_2^*| + |\alpha_2^*||\alpha_1|)$, $A_4 = \hbar U_{\mathrm{p}}$, $A_5 = \hbar U_1|\alpha_1|^2$ and $A_6 = \hbar U_2|\alpha_2|^2$. It is usual to express the potential amplitude in units of the recoil energy, defined

as $E_{\mathrm{r}} = \hbar^2 k_{\mathrm{r}}^2/2m$. The recoil energy is usually in the kHz range. The transverse pump lattice, at a wavelength of λ=785.3nm, has a depth of several recoils and we can notice that the strongest terms are the transverse pump and the pump-cavity terms. The recoil energy for this wavelength $E_{\mathrm{r}} = 2.3 * 10^{-30}$ J, which gives a recoil frequency of 2 $\pi\times$ 3.7 kHz. Using this value we obtain the coefficients in terms of recoils: $A_1 = A_2 = 0.48E_{\mathrm{r}}, A_3 = 0.087E_{\mathrm{r}}, A_4 = 1.34E_{\mathrm{r}}, A_5 = A_6 = 0.043E_{\mathrm{r}}$. A_1, A_2 and A_4 are the dominant terms, indeed when imaging the system the most visible points correspond to those scattered via these interactions, as will be shown later. The other terms contribute much less due to the fact that the cavity couplings are very weak.

The potential can be simulated with Mathematica or Python in real space to give the Figure 3.5, where the spatial coordinates have been rescaled by the wavelength λ. The pump phase ϕ determines the lattice geometry, when set to zero, the potential reveals a triangular geometry as shown in Figure 3.5. If the pump phase is

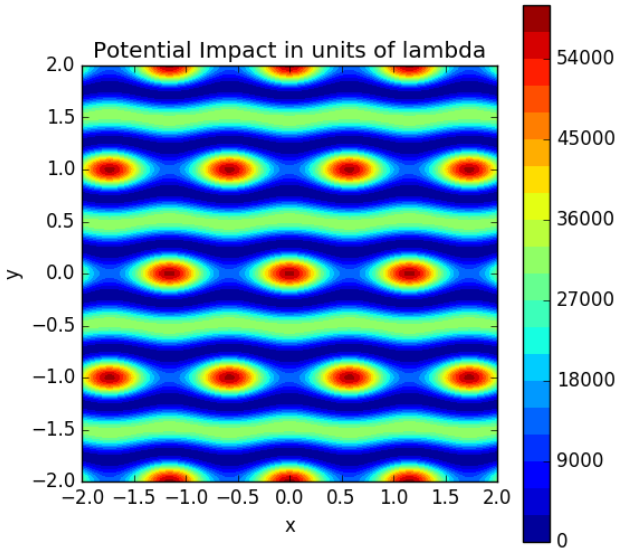

Figure 3.5: Triangular optical potential felt by the BEC atoms in the system with pump phase set to zero.

set to a value of $\pi/2$, the lattice geometry varies from triangular to hexagonal as shown in Figure 3.6.

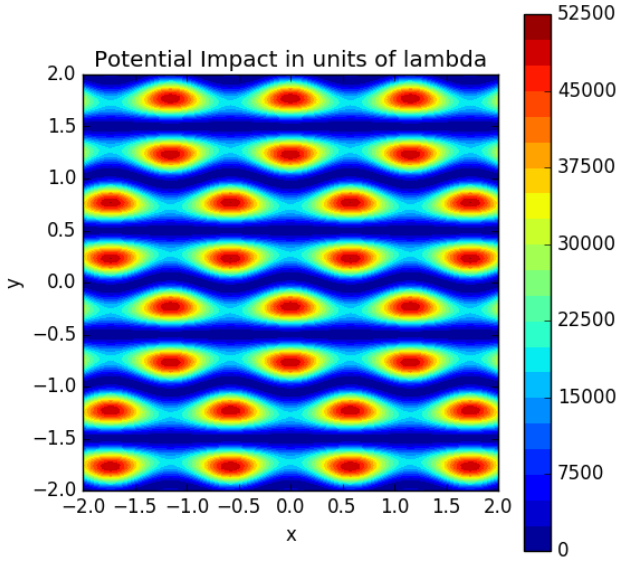

Figure 3.6: Hexagonal optical potential felt by the BEC atoms in the system with pump phase set to $\pi/2$.

The next step is to define a new basis, made of the wave vectors $\mathbf{k_p}$ and $\mathbf{k_1}$ in order to implement the Hamiltonian.

3.2.1 Hamiltonian implementation

In order to calculate the band structure, an existing Python code is adapted for the new lattice geometry. Calculating the band structure boils down to diagonalising the Hamiltonian for the system. Once we have the expression for the Hamiltonian, we need to come up with the corresponding matrix. To this aim we create a matrix whose diagonal elements correspond with the kinetic energy terms and whose off-diagonal elements correspond with the potential energy terms. In order to obtain the matrix elements we need to perform a Fourier Transform of the Hamiltonian terms from direct to reciprocal space. This means for example that we need to solve integrals of the form:

$$V_1(x,y) = \iint \Psi^\dagger(x,y)\hbar\eta_1(\hat{a}_1^\dagger + \hat{a}_2)\cos(\mathbf{k_p}\cdot\mathbf{r}+\phi)\cos(\mathbf{k_1}\cdot\mathbf{r})\Psi(x,y)dxdy, \tag{3.15}$$

The Hamiltonian matrix is a $N \times N \times N \times N$ tensor (where $N = 2n + 1$, n being the number of bands considered) whose indices correspond to the allowed scattering events, and to which we associate their weights. We refer to the code in the Appendix for more details. In the indices we encode the coordinates of origin and of end of each scattering event. Here we shift our basis coordinates from x and y to k_p and k_1, therefore each scattering event is rewritten in terms of these reciprocal lattice vectors only. Each term in the Hamiltonian identifies a specific allowed scattering event. While it is possible to choose a different basis for the scattering, we chose the basis formed by k_p and k_1 in order to capture both the transverse pump and cavity directions. Later sections will present an alternative basis.

The Hamiltonian, unlike the optical potential, is coded in reciprocal space. The Hamiltonian is then diagonalised and the eigenvalues are plotted to give the band structure. We first look at the lowest energy band for the kinetic energy alone in order to check our results.

3.2.2 Experimental verification

As discussed in previous sections, among all the scattering events, some have a larger amplitude and therefore are dominant. In particular, the cavity to pump and the pump standing wave terms are significantly larger than the others. This is demonstrated in the laboratory [3] by taking absorption images perpendicular to the cavity plane. First, the BEC is confined in a dipole trap, hence the attractive lattice from the transverse pump is created. Each cavity couples to the transverse pump proportionally to its coupling coefficients. By increasing these coefficients, a self-organised phase is reached beyond which the cavity modes are occupied homogeneously. By monitoring the photons leaking from the cavities, in situ monitoring of the system can be performed, and information about the ordering of the atoms deduced. Absorption images reveal the position of the atoms after the scattering events described in Figure 3.4. In particular the orange and yellow lines scattering are visible in Figure 3.7.

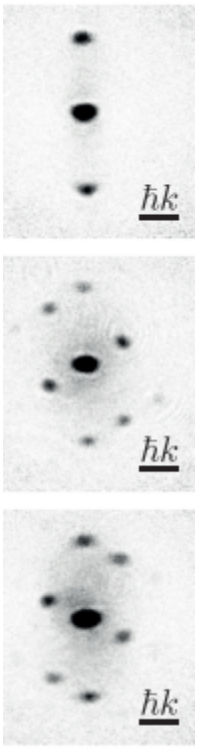

Figure 3.7: Absorption images showing the scattering events, from pump to pump and from cavities to pump. Figure taken from [3].

3.3 Band structure calculation

Calculating the band structure for the kinetic term only for the lowest four bands yields the result shown in Figure 3.8. Including also the potential term yields to Figure 3.9. This figure clearly shows an opening of the bands at the BZ boundary, as we would expect in the presence of a potential. Increasing the number of bands reveals the possible presence of Dirac points in the higher bands, in particular between the 4th and the 5th band.

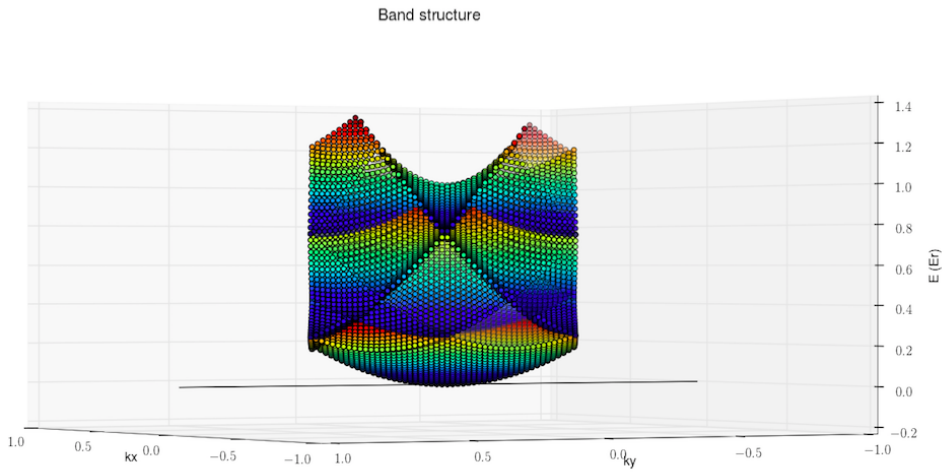

Figure 3.8: Band structure for kinetic term only.

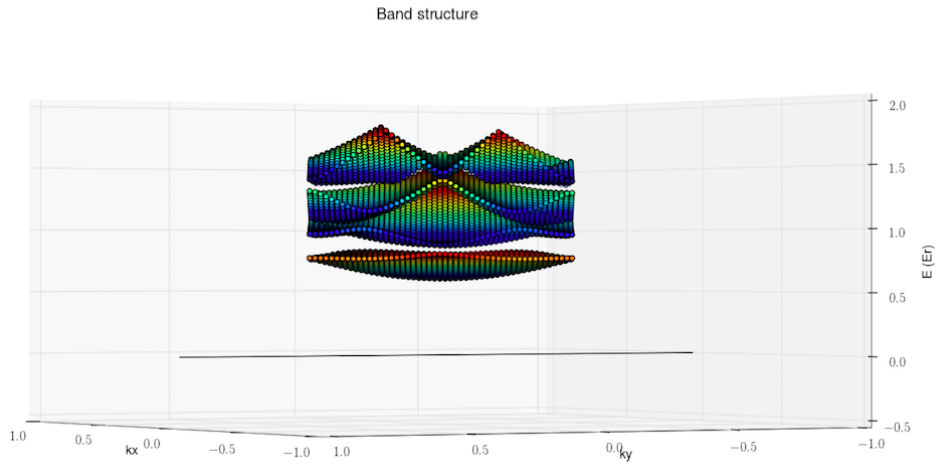

Figure 3.9: Lowest four bands structure for a Hamiltonian which includes the kinetic and the potential terms.

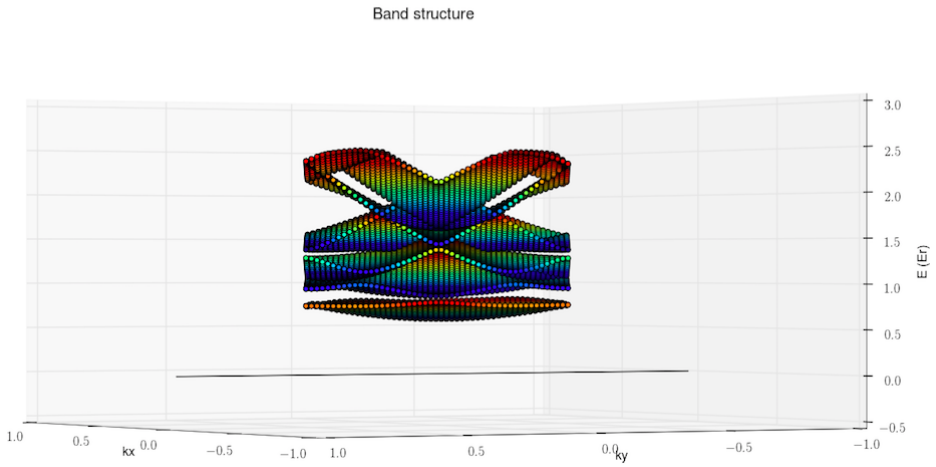

Figure 3.10: Lowest six bands structure for a Hamiltonian which includes the kinetic and the potential terms.

Note that the band structure calculation is carried out on a region of space spanned by the reciprocal lattice vectors k_{p} and k_1. This space corresponds to a partial section of the first BZ and a section of the second BZ, as shown in Figure 3.11. This can be verified by noting that the plotted space has the shape shown in Figure 3.11, rather than that of a unit cell, by calculating the lowest band kinetic term Hamiltonian and visualising it from above in a 2D plot.

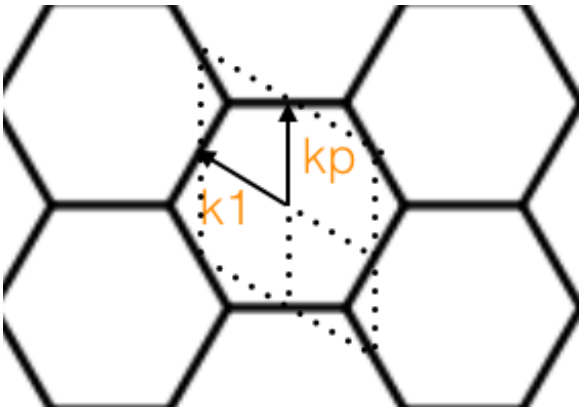

Figure 3.11: Space spanned by reciprocal vectors chosen as our basis for the calculation.

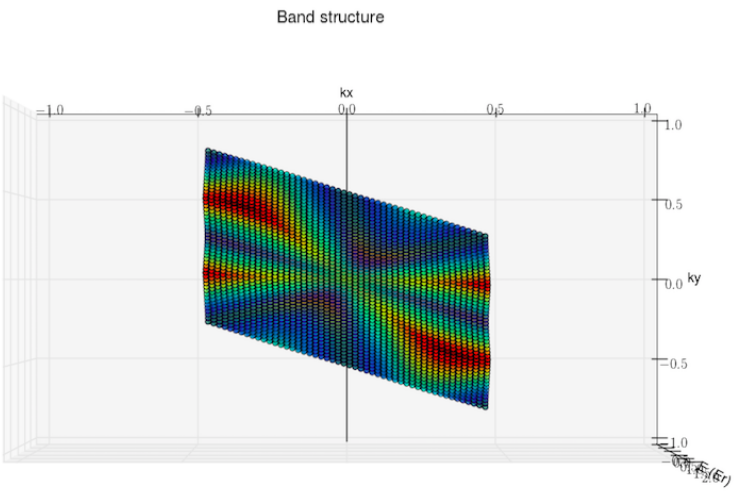

Figure 3.12: Space spanned by reciprocal vectors chosen as our basis for the calculation, top view of the band structure in reciprocal space.

In order to gain more intuition about the band structure and its significance, we

perform several studies based on the variation of the tunable parameters of the experiment. The system parameters, mentioned in previous sections, are the cavity coupling strengths g_1 and g_2, which are fixed by the cavity geometry, the coherent state amplitudes which quantify the light field in the cavities $|\alpha_1|$ and $|\alpha_2|$, the pump frequency Ω_{p} and the detuning Δ_a. As the cavity couplings are set by the cavity mode volumes, the main tunable parameters are the pump frequency and the light fields. Therefore we explore the band structure variation as these quantities are varied.

3.4 Exploring the band structure

The following section will present results relative to the exploration of the band structure when the experimental parameters are varied.

We are interested in exploring the variation of the band structure when the coherent state amplitudes $|\alpha_1|$ and $|\alpha_2|$ are varied form a balanced case ($|\alpha_1| = |\alpha_2|$) to an unbalanced case, while maintaining the sum of their squares constant, *i.e.* maintaining the total light field constant. The meaning of α is indeed a quantification of the light field present in each cavity, therefore an unbalanced case would correspond to a case with more light in one of the two cavities. This scenario can also be checked by studying the optical potential for the different values of the field. We begin with the current experimental situation with $|\alpha_1| = |\alpha_2| = 10$ and $|\alpha_1|^2 + |\alpha_2|^2 = 200$. Varying the values of α up to the extremum of the unbalanced situation with $|\alpha_1| = 2$ and $|\alpha_2| = 14$ and viceversa. The variation of potential and bands for the extreme cases is illustrated in Figure 3.13 and 3.14.

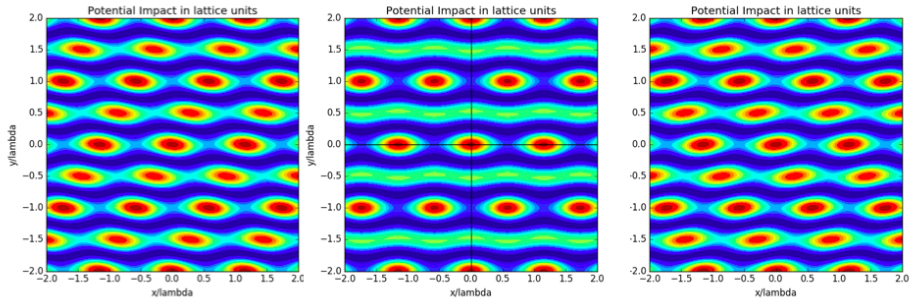

Figure 3.13: Variation of the potential for $|\alpha_1| = 2, |\alpha_1| = 10, |\alpha_1| = 14$.

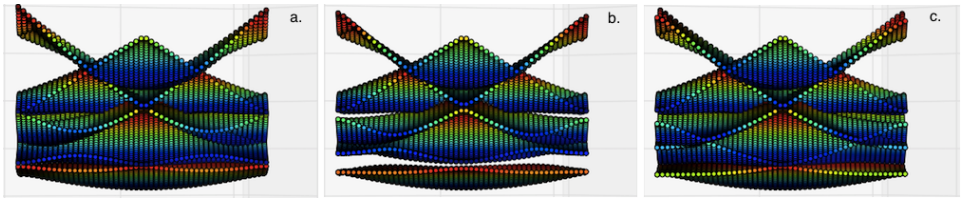

Figure 3.14: Variation of the five lowest bands for $|\alpha_1| = 2(a.), |\alpha_1| = 10(b.), |\alpha_1| = 14(c.)$. The axis have been omitted for visualisation purposes, but are the same as in Figure 3.9.

The figure shows that in the extreme unbalanced cases a gap closes on one side of the calculated area, whereas it is fully open when the light fields are balanced.

Next we are interested in studying how the band structure changes at the variation of the pump phase ϕ, which corresponds to the position of the retroreflecting mirror. Again, we start by analysing the variation of the optical potential and we then analyse the corresponding band structures. Similarly to the case of the light field variation, changing the pump phase corresponds to shifting the geometry of the potential which transforms from a hexagonal lattice to a triangular lattice. Both of these scenarios involve a modification of the type of optical lattice, resulting from the interfering standing waves. The potential is therefore strongly modified and we note that the most noticeable effect is on the gap between the first and second band. When varying the pump phase, the effect is a very slight increase of the band gap between the first and second bands for increasing angle. This means that the current triangular geometry has a smaller band gap than the hexagonal geometry.

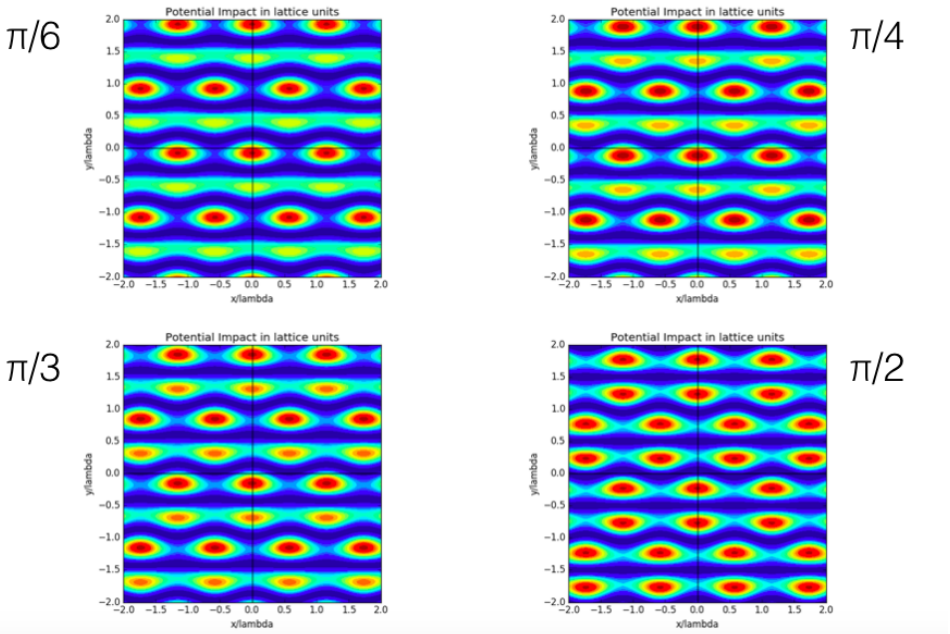

Figure 3.15: Variation of the potential for indicated values of the pump phase ϕ.

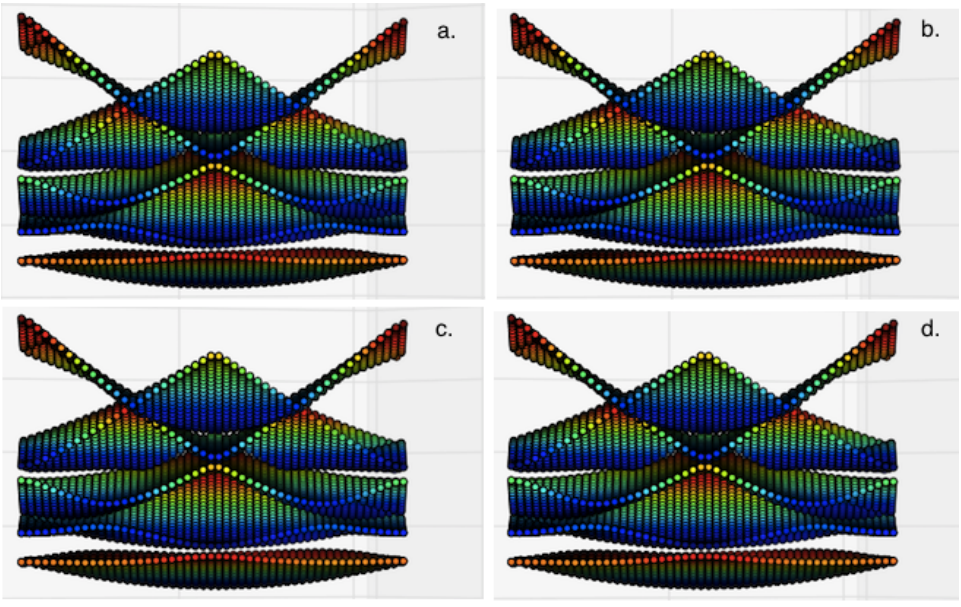

Figure 3.16: Variation of the bands for clockwise values of $\phi = \pi/6(a.), \pi/4(b.), \pi/3(c.), \pi/2(d.)$.

Finally we study the variation of the bands as a function of the strength of the potential terms, expressed by the coefficients $A_1, A_2, A_3, A_4, A_5, A_6$. Again, the tunable quantities are the light field α and the pump frequency Ω_p. In particular we study how the bands and the potential vary as the ratio between the coefficients A_1, A_2 and A_4 is changed. These three terms correspond to the pump-cavity and pump alone scatterings, as described in earlier sections. These are the dominant scattering terms due to the magnitude of the pump frequency relative to the cavity coupling rates g_2 and g_2. Since all these terms depend on Ω_p, we study the behaviour of the coefficients as Ω_p is varied. Figure 3.16 shows that while A_1 and A_2 vary in a linear way with Ω_p, A_4 varies in a quadratic fashion. Therefore there is only one point at which the coefficients are in a 1:1 ratio. This corresponds with $A_1 = A_2 = A_4 = 0.17E_r$ for $\Omega_p = 2\pi \times 36$ MHz. The ratio is varied from a

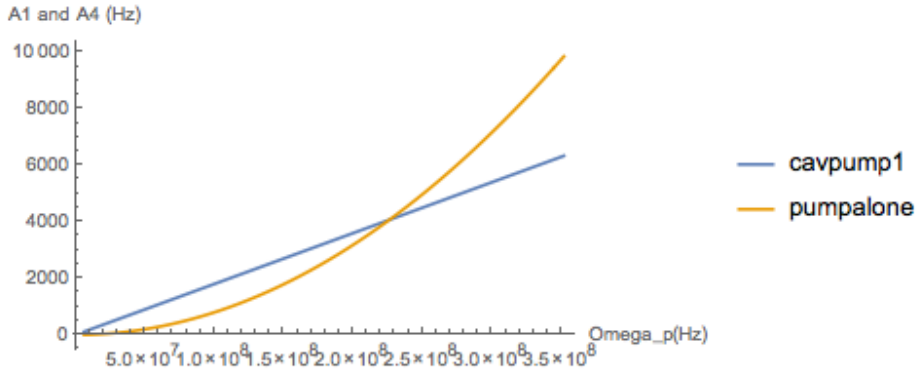

Figure 3.17: Coefficients A_1 and A_4 as a function of pump frequency Ω_p.

value of 1 to a value of 2.8, which corresponds to the current laboratory value of $\Omega_p = 2\pi \times 100$MHz. The values explored are: A_4/A_1= 1(a), 1.5(b), 2(c), 2.5(d), 2.8(e) in Figure 3.18. In this case what is varying is the amplitude of the potential, or in other words, the intensity of the potential, not its structure. We expect that the potential maintains the same geometry, but gets deeper or shallower. Indeed Figure 3.18 reveals the expected feature. We also see that, as the ratio increases for a stronger pump coefficient, the potential gets more squeezed along one direction, although in the same position.

This causes the richest variation of the band structure. Not only the lowest two bands, but also the higher bands, are noticeably modified . As the pump coefficient

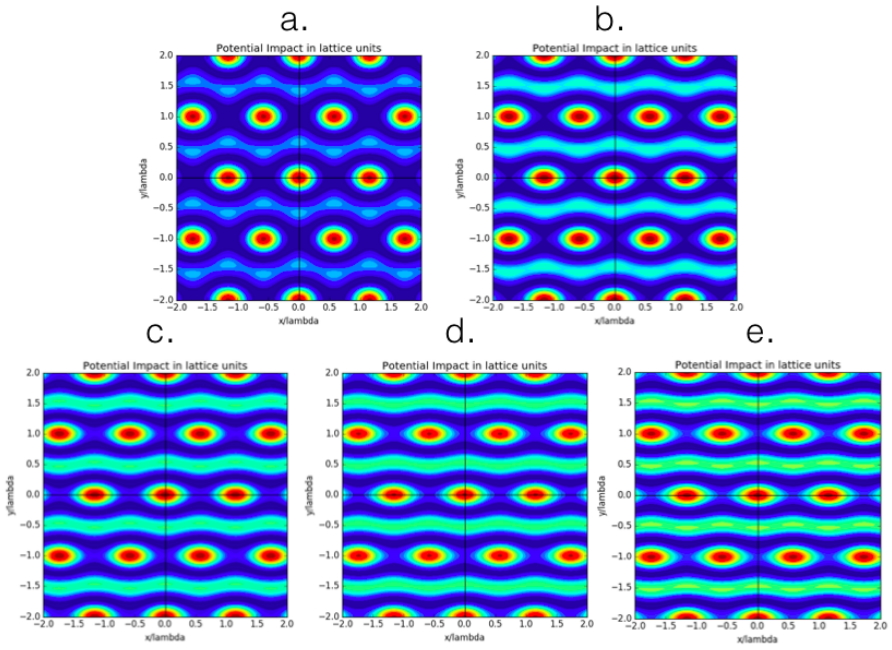

Figure 3.18: Optical potential variation for different ratios of pump to cavity coefficients.

increases, the gap between first and second band enlarges, but the one between bands three and four closes. The higher bands also show remarkable changes. An interesting development would be to be able to probe the band structure experimentally since being able to study the band structure of a system reveals information about its symmetries and properties. In particular the interest would be in the presence of Dirac points in the higher bands. Further studies are required in order to identify with precision the Dirac points, their location and how they are affected by changing the tunable parameters. In particular a plot showing a cut through the band structure along a particular reciprocal lattice vector direction would be helpful in identifying the Dirac points.

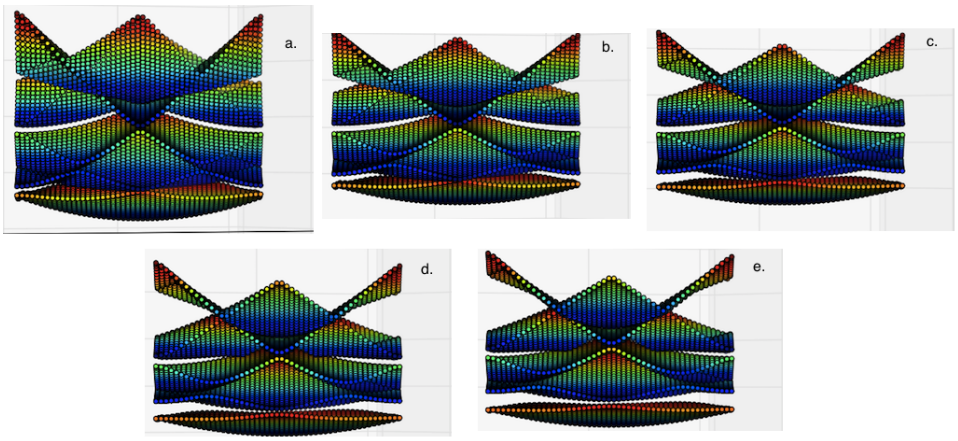

Figure 3.19: Band structure variation for different ratios of pump to cavity coefficients.

3.5 Alternative basis

When carrying out the calculation, different basis can be chosen. The peculiarity of the setup is that the pump and cavities are not orthogonal to each other. This makes it harder to calculate and depict the band structures. In order to capture the physics for the important directions, reciprocal lattice vectors along the cavities and pump direction are chosen. These directions are specified by equation (3.9). The three vectors are linked by equation (3.10). It is then possible to choose a cavity-pump basis, like the one that has been presented so far, made up of the vectors k_{p} and k_1 at 60 °, or to choose a cavity-cavity basis, with k_1 and k_2 as the reciprocal lattice vectors, at 120 °. The difference introduced by the choice of basis lies in the space over which the Hamiltonian diagonalisation is carried out. In the pump-cavity basis, this space is spanned by k_1 and k_{p} and is shown in Figure 3.10, whereas for the cavity-cavity basis this space corresponds to that shown in Figure 3.20.

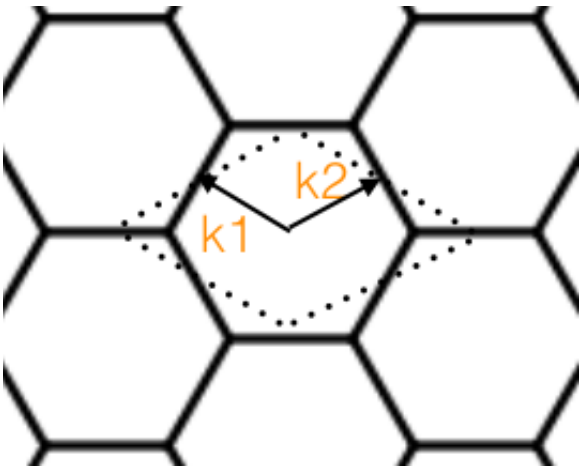

Figure 3.20: Space of calculation for the cavity-cavity basis.

Both these spaces include parts of the adjacent Brillouin Zones and parts of the first BZ are not included. However some high symmetry points are present in both basis spaces. At the corresponding angles of 150° and 270°, the band structures can be compared and indeed show the same features, as illustrated by Figure 3.22 and 3.23.

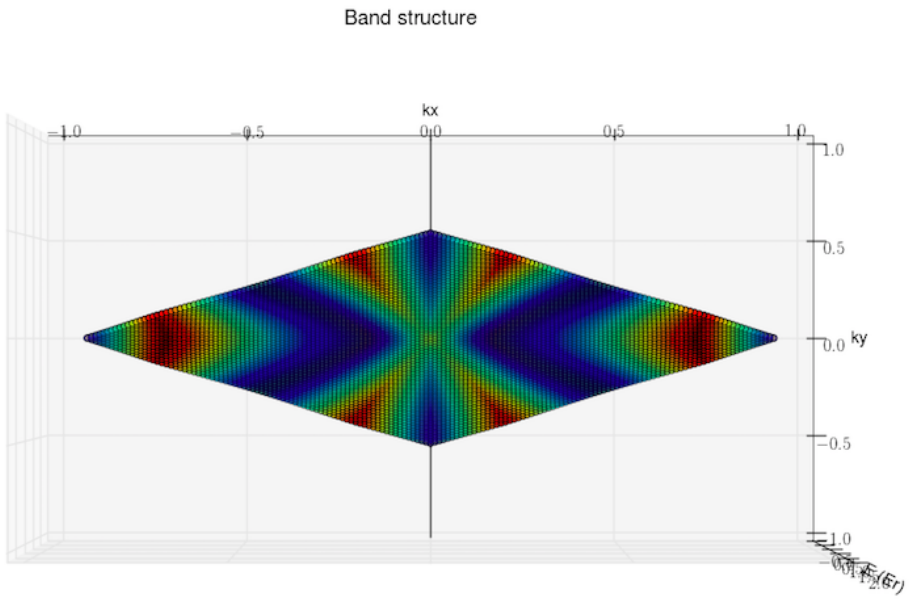

Figure 3.21: Space of calculation for the cavity-cavity basis.

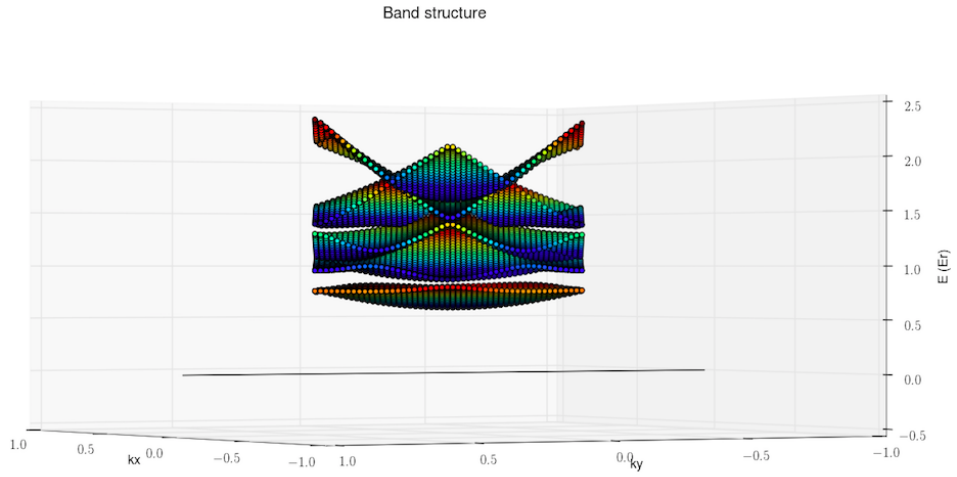

Figure 3.22: View from an angle of 150° of the band structure as calculated in the cavity-pump basis.

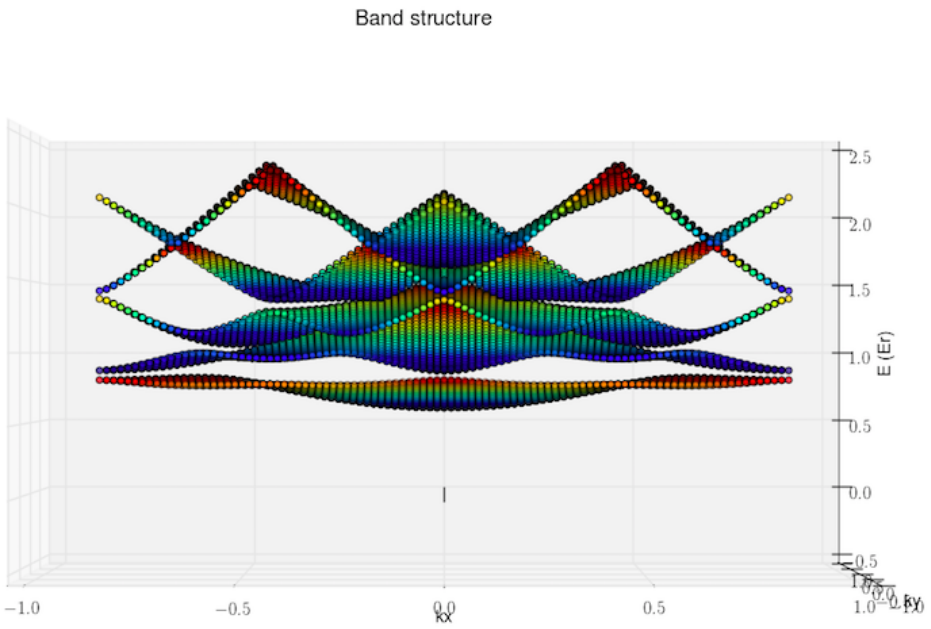

Figure 3.23: View from an angle of 270° of the band structure as calculated in the cavity-pump basis, a 120° shift shows the same points in the BZ.

3.6 Conclusion

This band structure calculation was performed in the attempt of sheding light on the fundamental structure of the system of a BEC confined in a dipole trap and sitting on a lattice formed by the interference between the transverse pump lattice and the cavities lattice. We have obtained the band structure by considering the Hamiltonian in a specific basis given by the non orthogonal reciprocal lattice vectors. Diagonalisation of the Hamiltonian was performed in Python in order to obtain the eigenenergies, corresponding to the allowed energy values for the system. Plotting the band structure for the kinetic energy alone results in a gapless dispersion relation while including the potential term opens gaps, as expected. The band structure is explored by varying the experimentally tunable parameters, namely the coherent field amplitudes, the transverse pump frequency and the transverse pump phase. Modifying these parameters results in noticeable changes in the bands, in particular involving the lower energy bands. Further investigation is required in order to better identify possible Dirac points in the higher energy bands and to fully characterise the bands.

In this work I have described the results of my master thesis at ETH Zurich performed in the spring and summer 2016. I have focused on the topic of quantum simulation with BEC. The thesis consisted of two projects, both closely related and concerned with quantum optics experiments at ETH. I have chosen, despite my experimental background, to perform a theoretical master thesis in order to experience a different way of thinking and in order to go beyond my comfort zone. Indeed, these months have proven to be quite challenging, at the same time I have learned many precious skills. I enjoyed both topics very much and had the chance to revisit area of physics which I had not worked on in the past few years. Yet, both projects were heavily involved with the field of Quantum Optics, in which I wish to work in the future.

Appendix

This appendix contains the source codes for both the projects. The first project is written in Matlab, the second project in Python. The reason for this is that the second code is adapted from an existing file (specifically, potential.py and constants are the adapted files).

It also contains a brief account of an experimental work carried out as a voluntary project at ICFO, Barcelona, in the spring 2016 within the Europhotonics Masters programme. The experimental work aim was to design and assemble a cavity for PDH stabilisation of an Infrared laser.

Appendix A

Cavity design for laser stabilisation

The previous chapters have focused on the theoretical work pursued at ETH over six months. Both research lines converged on understading fundamental behaviour of a BEC when confined in high finesse optical cavities. Right before commencing my theoretical adventure, I worked on a personal experimental project at ICFO near Barcelona for two months. My project was coincidentally concerned with designing, assembling and aligning a high finesse optical cavity. Since optical cavities have been at the backbone of my master thesis work, I have decided to include this chapter to give an account of my experimental work at ICFO, which hopefully introduces a nice experimental touch to the thesis.

A.0.1 Motivation

My experimental work at ICFO was performed in the QPSA (Quantum Photonics with Solids and Atoms) group led by Prof. Hugues de Riedmatten. The group researches different implementation of quantum memories for quantum information transport and storage [50]. In particular, I joined the solid state quantum memory team.

The need for quantum memories stems from quantum information protocols such as entanglement swapping and teleportation. Quantum information is usually transferred using optical fibres, which have characteristic losses, for this reason it is necessary to establish links called *quantum repeaters* along the transfer line. Quantum memories have the ability to store quantum information and release it on demand. Several types of quantum memories exist, such as atomic ensembles, nitrogen vacancy centres in diamond, quantum dots: each of them comes with their relative advantages and disadvantages. One of the most promising type of quantum memory is indeed a solid state quantum memory.

Solid state quantum memories are rare-earth doped crystals which are cooled to cryogenic

temperatures (around $\simeq$ 5-10 K). Rare earth ions have a peculiar energy structure which allows a shielding from the surrounding lattice structure, thus allowing long coherence times. Usually the interactions of the ions with the lattice structure is strong enough that the coherence times are overall very short. Rare earth ions are a fortunate exception. When cooled to cryogenic temperatures, the main broadening mechanism is inhomogeneous broadening due to the inhomogeneous distribution of the ions in the crystal. In order to store quantum information in the memory, the quantum information is encoded as a quantum state on a single photon. The single photon is then coupled to the memory where the quantum state is stored and then retrieved. Recently a protocol has been developed which allows storage and on demand retrieval of the quantum information: the atomic frequency comb (AFC) protocol [51]. The protocol requires a laser shone to the crystal as a write and a read beam. In order to increase the storage time and to obtain a memory with higher efficiency and fidelity, the stability of the write and read laser is crucial.

My work was focused on building an optical high finesse cavity in order to stabilise the master laser. The stabilisation was done following the Pound-Drever-Hall (PDH) technique [52]. The following sections will describe the main steps to creating a working cavity for laser stabilisation. These are: the cavity design, the cavity assembly, the temperature stabilisation, shining light through the cavity, finding the fundamental mode of the cavity and finally aligning the cavity.

A.0.2 Design and Assembly

The master laser of the solid state memory experiment is an infrared laser at λ=1212 nm. Currently, this laser is stabilised via PDH technique to a cavity after having been frequency doubled to a wavelength of 606 nm which is the wavelength used in the experiment. In order to optimise the stability, it is proposed to create a new cavity at 1212 nm and to stabilise the laser directly at the source and not after it having been double frequenced. The new cavity will replace the old cavity in the existent vacuum chamber. The design of the cavity therefore has the constraint of the dimensions of the vacuum chamber, otherwise it has no specific constraints. The old cavity is 15 cm long, we decide to gain in length and make the new cavity 17 cm long. Hence the free spectral range of the cavity will be modified from 1 GHz to 0.88 GHz according to $\Delta_{\mathrm{FSR}} = \frac{c}{nL}$, where c is the speed of light, n the refractive index and L the length of the cavity. A finesse of $F =\simeq$ 800 (in vacuum) is expected. The design of the cavity is carried out using Inventor and assembled on the optical table. The holding cube is in aluminium, as the cavity tube. The inner spacers are made of teflon and rubber. At the end of the tube the teflon spacers hold the two mirrors, one of them is attached to three piezo motors which allow scanning of the cavity in order to find the fundamental mode. Below the design of the cavity is shown:
The total length of the cavity, considering the cavity tube and the cavity cap, is of 192 mm. Once the design is created, the cavity is assembled on the optical table. In between the cavity tube and the holding cube two Peltiers are inserted which are used for the temper-

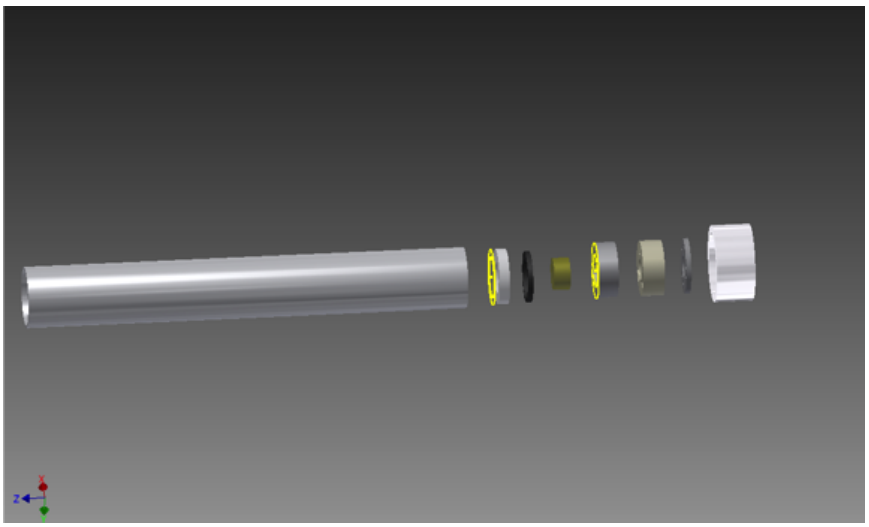

Figure A.1: Inventor design for the high finesse cavity, inside view.

ature stabilisation. It is important to have a stable temperature inside the cavity to ensure the minimisation of mode fluctuation inside the cavity.

A.0.3 Temperature stabilisation

The temperature stabilisation is perfomed using two Peltiers. These are flat semiconductor structures made of two plates p and n-doped respectively. Upon current transfer through the Peltier, one of the plates heats up and the other cools down, due to the displacement of the charge carriers when a temperature gradient is present. This system exploits the themoelectric effect to convert temperature differences to electric voltage differences and viceversa. Thermoelectric devices are used as temperature controllers due to the ability to monitor and change temperature or voltage. We study the temperature fluctuations of the cavity by inserting the Peltiers and exploring the amplitude of the voltage fluctuations for different resistors ratios on the Peltiers module. We then fix the temperature at 30 $^\circ$ C, for values of the resistors of R_{p}=6 MHz and R_{I}=121kHz. This temperature corresponds to an electric voltage of V=1.242 V. In general, it is common practice to stabilise a cavity to a temperature slightly above room temperature.

A.0.4 Alignement

Once the cavity is assembled and temperature stabilised, light is ready to be injected. The light comes from a secondary port of the master laser at 1212 nm. It has to be fibre coupled from the master laser to the other side of the optical table where the cavity is placed. With a powermeter we check the power at the master laser port. The power at the port is of 10mW. Two mirrors are used to direct the light into the incoupling fibre, as the mirrors are lossy,

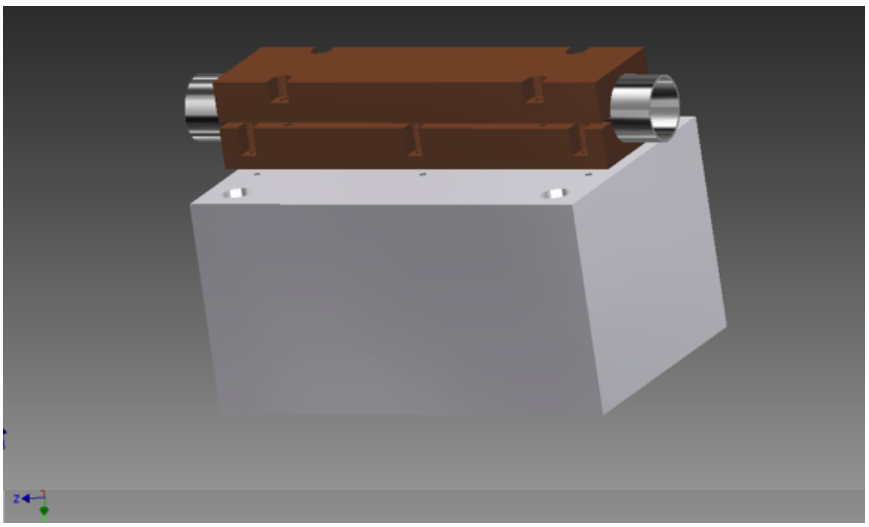

Figure A.2: Inventor design for the high finesse cavity, outside view.

after reflection we have a power of 9mW. We discover that Thorlabs produces mirrors with high reflective coating up to 1100nm, our wavelength of 1212 nm is outside this range. For this reason we try to optimise the incidence and reflection angle of the light on the mirrors (when the angle is closer to the normal, the reflectivity is higher). We then fibre couple the light, after which at the outcoupler we have a power of 2mW. We aim at injecting a large portion of this power into the cavity. From the outcoupler, the light goes through a collimating lens and several optical devices are inserted along its path before reaching the cavity entrance port. This is because we need to monitor the light going through the cavity mirrors (transmission) and the light being reflected by the cavity mirrors (reflection) using Avalanche Photodiodes (APDs), therefore we need to insert a Polarisation Beam Splitter (PBS) cube which lets through light of a particular polarisation and reflects light of the orthogonal polarisation. Figure A.3 shows the optics inserted between the fibre outcoupler and the cavity.

The light from the outcupler goes through a collimating lens, a half-wavelength plate which allows only linearly polarised light to pass through, a PBS through which all of the light goes, three mirrors to direct the light towards the cavity, a quarter-wave plate which converts linearly polarised light to circularly polarised light. Light incident on the cavity gets trasmitted and reflected. The reflected light will go through the optical elements and will be reflected by the PBS and directed to an APDs which monitors the reflection of the cavity. After the cavity, an APD and an infrared camera are inserted in order to monitor the trasmission of the cavity and to visualise the cavity modes.

In order to find the fundamental mode and to optimise for it, it is crucial to have a beam diameter incident upon the cavity which matches the cavity gaussian mode diameter. As-

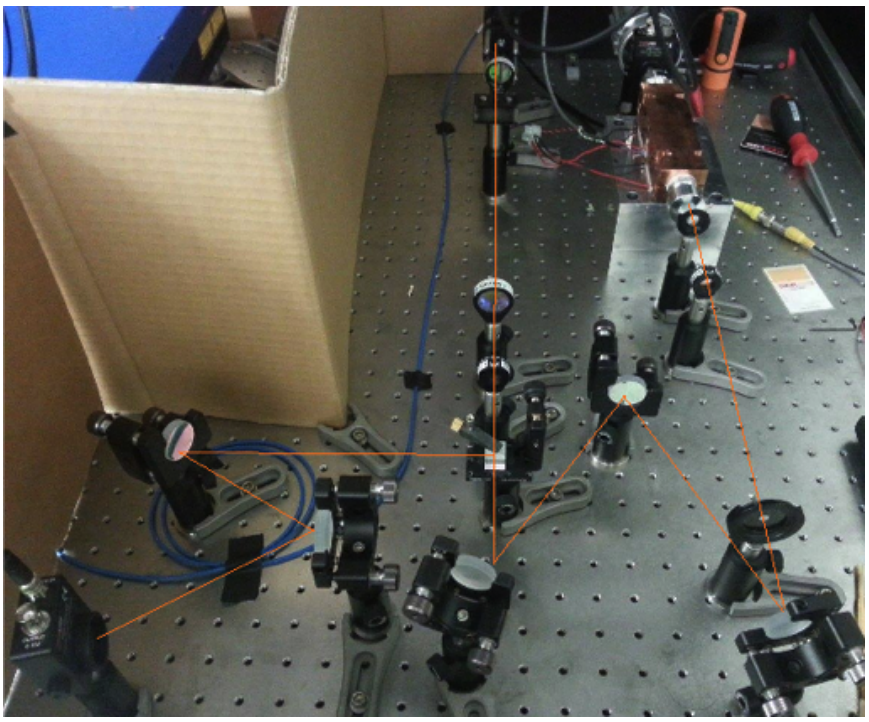

Figure A.3: Optical system for laser stabilisation via high finesse cavity.

suming that the cavity sustains a perfect gaussian mode with the wist at the center of the cavity, it is possible to calculate the theoretical diameter of the beam at the entrance mirror of the cavity. Therefore it is then possible to match the dimension of the collimated beam produced by the collimating lens after the optical fibre outcoupler to this theoretical diameter. This can be done by using a collimating lens of different focal length and also by inserting a telescope along the path.

As we did not have an infrared camera, we decided to try to construct one from a commercial security night camera. We removed the LEDs and left the CCD camera. We then connected the IR camera to a commercial monitor and aligned it to the cavity trasmission light in order to visualise the modes. To see the modes, we scan the cavity via the Piezo drivers attached to one end of the cavity. The piezos are connected to a module via which we can modify the scanning amplitude and frequency of the cavity. Scanning the cavity means modifying slightly the length of the cavity in order to find the resonance condition and the fundamental mode. This was done combining the use of the camera to visualise the fundamental mode and the APD in order to make sure the visualised mode was effectively the fundamental. A picture of the fundamental mode is shown in Figure A4. Once the fundamental mode is found, a beam walk technique is used on the coupling mirrors to

Figure A.4: Fundamental mode of the cavity.

optimise the alignment of the cavity. At the end of the alignment the cavity is not scanned anymore and it is fixed to position. The aligned cavity is then ready to be moved inside the vacuum chamber and to substitute the old cavity. This concludes the brief experimental project carried out in the QPSA group at ICFO.

Appendix B

Collapse and revival

The results presented for the collapse and revival project are generated using Matlab codes. There are several source files, which include either only short range interaction, short and long, tunnelling and which calculate the evolution of the order parameter for a system of one or four sites for a different number of particles (two, three, four). Most of the results come from considering 4 sites and up to 2 particles per site. We don't include all variations of the code, but only a sample for a code generating the evolution with short range interactions only, and one for short and long interactions. Extra codes were also produced to study a pump-probe scenario which is not included in this thesis.

```
clear all
close all
clc

% evaluating <a> in the Heinseberg picture <phi|a(t)|phi>
    with
% a(t)=e^iHt/h_bar*a*e^-iHt/h_bar
% defining the Hamiltonian which contains the on-site
    interaction term and
% the long range term depending on the imbalance even/odd
    sites
% restrict to a square lattice of 4 total sites (2 x 2)
% Hamiltonian H=sumi U/2 n_i(n_i-1) - Ul/k (sume n_e - sumo
    n_o)^2
% define fock basis and number state matrix

I = eye(3);
nsi = [0 0 0; 0 1 0; 0 0 2];
nsi2 = nsi*(nsi-I);
```

```
% short range hamiltonian
% I am breaking the hamiltonian on each site and then
    summing them.
% applying the hamiltonian on a site include applying
    identity operators on
% all other sites therefore the hamiltonian is a tensorial
    product

U = 2150;
H1 = (U/2 .* (kron(nsi2,kron(I,kron(I,I)))));
H2 = (U/2 .* (kron(I,kron(nsi2,kron(I,I)))));
H3 = (U/2 .* (kron(I,kron(I,kron(nsi2,I)))));
H4 = (U/2 .* (kron(I,kron(I,kron(I,nsi2)))));

Hshort = H1+H2+H3+H4;

a1 = [0 sqrt(1) 0; 0 0 sqrt(2); 0 0 0];
a= kron(a1,kron(I,kron(I,I)));

t = 0:0.00001:0.01;
alpha = 1;
l = 2;

hbar=1
ketcs_tot =
    kron(ket_coherent(alpha,l),kron(ket_coherent(alpha,l),
kron(ket_coherent(alpha,l),ket_coherent(alpha,l))));
overlap = ket_coherent(alpha,l)'*ket_coherent(alpha,l)
cstot = 1/sqrt(overlap) .* ket_coherent(alpha,l);
normcheck = cstot'*cstot
csnorm = kron(cstot,kron(cstot,kron(cstot,cstot)));



%%
    for ti=1:length(t)
         at(ti) = csnorm'*(expm(1i*t(ti)*Hshort)*a*
         expm(-1i*t(ti)*Hshort))*csnorm;
    end
```

```
plot(t,abs(at).^2)
[pks,locs] = findpeaks(abs(at).^2)


title('Collapse and revivals with on site interactions only
    with 2 atoms')
 xlabel('t [hbar/U]')
ylabel('|<a>|^2')
```

```
clear all
close all
clc

% evaluating <a> in the Heinseberg picture <phi|a(t)|phi>
    with
% a(t)=e^iHt/h_bar*a*e^-iHt/h_bar

% defining the Hamiltonian which contains the on-site
    interaction term and
% the long range term depending on the imbalance even/odd
    sites

% restrict to a square lattice of 4 total sites (2 x 2)
% Hamiltonian H=sumi U/2 n_i(n_i-1) - Ul/k (sume n_e - sumo
    n_o)^2
% define fock basis and number state matrix

I = eye(3);
nsi = [0 0 0; 0 1 0; 0 0 2];
nsi2 = nsi*(nsi-I);


% short range hamiltonian
% I am breaking the hamiltonian on each site and then
    summing them.
% applying the hamiltonian on a site include applying
    identity operators on
% all other sites therefore the hamiltonian is a tensorial
    product

U = 775;
```

```
H1 = (U/2 .* (kron(nsi2,kron(I,kron(I,I)))));
H2 = (U/2 .* (kron(I,kron(nsi2,kron(I,I)))));
H3 = (U/2 .* (kron(I,kron(I,kron(nsi2,I)))));
H4 = (U/2 .* (kron(I,kron(I,kron(I,nsi2)))));

Hshort = H1+H2+H3+H4;

% Long range interactions differentiate between even and
    odd sites. I
% assign s1, s3 =odd s2,s4=even, however ns1=ns2=ns3 etc =
    nsi, but the
% important point is the order of the kronecker product


Ul = 0;

%U_{\rm l}=325;
k=1;
n1 = kron(nsi,kron(I,kron(I,I)));
n2 = kron(I,kron(nsi,kron(I,I)));
n3 = kron(I,kron(I,kron(nsi,I)));
n4 = kron(I,kron(I,kron(I,nsi)));

Hlong = -Ul/k .* mpower(((n2+n4)-(n1+n3)),2);

% total hamiltonian H = Hshort+Hlong
Htot = Hshort + Hlong;


% creation and annihilation operators in fock basis defined
    above for the
% space of the hamiltonian (81x81)
a1 = [0 sqrt(1) 0; 0 0 sqrt(2); 0 0 0];
a= kron(a1,kron(I,kron(I,I)));

%wavefunction
alpha = 1;
l = 2;
ketcs_tot =
    kron(ket_coherent(alpha,l),kron(ket_coherent(alpha,l),
kron(ket_coherent(alpha,l),ket_coherent(alpha,l))));
```

```
overlap = ket_coherent(alpha,l)'*ket_coherent(alpha,l);
cstot = 1/sqrt(overlap) .* ket_coherent(alpha,l);
normcheck = cstot'*cstot;
csnorm = kron(cstot,kron(cstot,kron(cstot,cstot)));

t = 0:0.0001:0.1;

   for ti=1:length(t)
        at(ti) = csnorm'*(expm(1i*t(ti)*Htot)*a*
        expm(-1i*t(ti)*Htot))*csnorm;
   end

plot(t,abs(at).^2)
hold on

U1=0
H11 = (U1/2 .* (kron(nsi2,kron(I,kron(I,I)))));
H21 = (U1/2 .* (kron(I,kron(nsi2,kron(I,I)))));
H31 = (U1/2 .* (kron(I,kron(I,kron(nsi2,I)))));
H41 = (U1/2 .* (kron(I,kron(I,kron(I,nsi2)))));
Hshort1 = H11+H21+H31+H41;
Ul1 = 77.5
Hlong1 = -Ul1/k .* mpower(((n2+n4)-(n1+n3)),2);
Htot1 = Hshort1 + Hlong1;

for ti=1:length(t)
        at1(ti) = csnorm'*(expm(1i*t(ti)*Htot1)*a*
        expm(-1i*t(ti)*Htot1))*csnorm;
   end

plot(t,abs(at1).^2, 'r')

%finding the peaks of the function and their location
%fitting the oscillating decay trend with an exponential
   function

[pks,locs] = findpeaks(abs(at).^2)

%fit = fit(locs'.*0.00001,pks','exp1')
%plot(fit,locs'.*0.00001,pks')
```

```
title('Collapse and revivals with interactions
    superimposed')
xlabel('t [hbar/U]');
%xlabel('t $\hbar$,interpreter,latex /U ')
ylabel('|<a>|^2')
```

Appendix C

Band structure calculation

The band structure calculation is handled by four main files: constants, where the constants are defined and the coefficients can be calculated for any configuration, potential, where the potential is defined as PotentialImpact, bands where the Hamiltonan is defined, diagonalized and the eigenenergies are plotted in the cavity-pump basis, and bands2 which is equivalent to bands but for the cavity-cavity basis. The following includes the first three files, we omit the last one has it is equivalent to bands.py except for the definition of the reciprocal lattice vectors.

```
# -*- coding: utf-8 -*-
#band structure calculation for the impact experiment, plot
    of the potential and of the first n bands in space
    spanned by the reciprocal lattice vectors
#created by Chiara Decaroli, Sept 2016

import numpy as np
import matplotlib.pyplot as plt
from mpl_toolkits.mplot3d import Axes3D
import matplotlib
from numpy.linalg import eigvalsh as solver
from math import pi
import potential
from matplotlib import cm


#POTENTIAL
#plotting the potential, all values can vary, coefficients
    in units of recoils, the coefficients Ai are found in
    the constants.py file
```

```
#the potential is defined in potential.py

A1,A2,A3,A4,A5,A6, phi = (0.483539994114, 0.483539994114,
    0.0870371989405, 1.34316665032, 0.0435185994703,
    0.0435185994703, pi/3)

potfig = potential.PotentialImpact(A1,A2,A3,A4,A5,A6,phi)
potfig.draw(show_bonds=False, show_diagonals=False,
    show_sections=False, save=True)
plt.title('Potential Impact in lattice units')
plt.xlabel('x/lambda')
plt.ylabel('y/lambda')
plt.plot((-2, 2), (0, 0), 'k-') #shows a line going through
    [0,0]
plt.plot((0, 0), (-2, 2), 'k-')
plt.show()

#HAMILTONIAN
#hamiltonian definition

def Hamiltonian(p1,p2,n0):
   N=2*n0+1

   #A1,A2,A3,A4,A5,A6,phi = (0,0,0,0,0,0,0) #for kinetic
      term only
   A1,A2,A3,A4,A5,A6, phi = (0.483539994114,
      0.483539994114, 0.0870371989405, 1.34316665032,
      0.0435185994703, 0.0435185994703, 0) #by taking a
      recoil of 23kHz with wrec=hbark^2/2m, pot in units
      of recoil, can check these values in the file
      constants.py

   H=np.zeros((N,N,N,N),'complex')
   q1,q2,q3,q4=np.indices(H.shape)

   #diagonal elements = kinetic terms
   H+=np.where((q1==q3) & (q2==q4), (p1+(q1-n0))**2+
   (p2+(q2-n0))**2+2*np.dot(K1,K2)*(p1+(q1-n0))*(p2+(q2-n0)),
      0)

   #pump-cav1
```

```
H += np.where((q3-q1==1) & (q4-q2==1),
    A1*0.25*np.exp(1j*phi),0)
H += np.where((q3-q1==1) & (q4-q2==-1),
    A1*0.25*np.exp(1j*phi),0)
H += np.where((q3-q1==-1) & (q4-q2==1) ,
    A1*0.25*np.exp(-1j*phi),0)
H += np.where((q3-q1==-1) & (q4-q2==-1) ,
    A1*0.25*np.exp(-1j*phi),0)

#pump-cav2
H += np.where((q3==q1) & (q4-q2==1),
    A2*0.25*np.exp(1j*phi),0)
H += np.where((q3==q1) & (q4-q2==-1),
    A2*0.25*np.exp(-1j*phi),0)
H += np.where((q3-q1==2) & (q4-q2==-1),
    A2*0.25*np.exp(1j*phi),0)
H += np.where((q3-q1==-2) & (q4-q2==1),
    A2*0.25*np.exp(-1j*phi),0)

#cav1-cav2
H += np.where((q3-q1==1) & (q4==q2), A3*0.25,0)
H += np.where((q3-q1==-1) & (q4==q2), A3*0.25,0)
H += np.where((q3-q1==1) & (q4-q2==-2), A3*0.25,0)
H += np.where((q3-q1==-1) & (q4-q2==2), A3*0.25,0)

#pump
H += np.where((q3-q1==2) & (q4==q2),
    A4*0.25*np.exp(2*1j*phi),0)
H += np.where((q3-q1==-2) & (q4==q2),
    A4*0.25*np.exp(-2*1j*phi),0)
H += np.where((q3==q1) & (q4==q2), A4*0.25*2,0)

#cav1
H += np.where((q3==q1) & (q4-q2==2), A5*0.25,0)
H += np.where((q3==q1) & (q4-q2==-2), A5*0.25,0)
H += np.where((q3==q1) & (q4==q2), A5*0.25*2,0)


#cav2
H += np.where((q3-q1==2) & (q4-q2==-2), A6*0.25,0)
H += np.where((q3-q1==-2) & (q4-q2==2), A6*0.25,0)
```

```
    H += np.where((q3==q1) & (q4==q2), A6*0.25*2,0)


    return H.reshape(N**2,N**2)

#calculating bands - diagonalisation of the Hamiltonian

grid=50 #n° points in the figure
bands=5 #n° bands

K1=np.array([-np.sqrt(3.)/2,1./2]) #reciprocal lattice
    vectors kp and k1
K2=np.array([0,1])

k1s=np.linspace(-0.5,0.5,grid)#x and y values
k2s=np.linspace(-0.5,0.5,grid)
bottom=np.zeros((grid,grid,bands)) #z values
kvalues=np.zeros((grid,grid,2))


for i,k1 in enumerate(k1s):
    for j,k2 in enumerate(k2s):
        kvalues[i,j]=k1*K1+k2*K2
        bottom[i,j]=solver(Hamiltonian(k1,k2,5))[:bands]
            #diagonalisation of the Hamiltonian

k=kvalues.reshape(grid*grid,2)
bottom=bottom.reshape(grid*grid,bands)

#plotting
#full band structure 3D plot in space of calculation

fig=plt.figure(figsize=(25,25))
ax =fig.add_subplot(111, projection='3d')
ax.view_init(azim=150,elev=0) #elev 90:view from top, 0
    view from side
ax.set_xlim(-1,1) #sets the x and y limit on the graph
ax.set_ylim(-1,1)
ax.mouse_init() #rotates and zooms the figure with the mouse
ax.can_zoom()
```

```
for b in xrange(bands):
    ax.scatter(k[:,0],k[:,1],bottom[:,b],c=bottom[:,b])
    ax.set_xlabel('kx')
    ax.set_ylabel('ky')
    ax.set_zlabel('E (Er)')

plt.title('Band structure')
plt.plot((0,0 ), (1, -1), (0,0), 'k-') #line going through
    E=0
plt.show()

#band structure cut

fig2 = plt.figure()
ax2 = fig2.add_subplot(111)
for b in xrange(bands):
    ax2.plot(k[2451:2500,1],bottom[2451:2500,b]) #choose the
        range of the cut
ti = np.array([0,0.5]) #choose the axis ticks limits
matplotlib.rc('text', usetex=True)
my_xticks = ["$\Gamma$", 'M'] #name the high symmetry points
plt.xticks(ti, my_xticks)
ax2.set_ylabel('E (Er)')
#ax2.set_xlim(0,0.5) #sets the x and y limit on the graph
plt.show()
plt.title('Band structure cut')
```

```
#!/usr/bin/python

###
# Class 'Potential': define some lattice potential,
# measure some relevant quantities and plot the landscape
    in 2d
#PotentialImpact class added by Chiara Decaroli, sept 2016
###

import numpy as np
import matplotlib.pyplot as plt

from scipy import optimize
from math import pi
```

```
import sys
import time


def distance(x1,x2):
  return np.sqrt((x2[0]-x1[0])**2+(x2[1]-x1[1])**2)


class Potential():

  # To be implemented in child classes
  def potential(self, x, y):
    return 0

  # To be implemented in child classes
  def save_figure(self, name):
    pass

  # To be implemented in child classes
  def get_symmetry(self):
    return 1

  # Look for the potential minima, where the atoms should
     actually sit;
  # called during object initialisation; result is written
     in self.atom
  def find_minima(self):
    f = lambda ndarr: self.potential(ndarr[0],ndarr[1])
    x0 = [np.array([-0.5,0]),np.array([0.5,0])]
    self.atom = []
    for i in range(2):
      self.atom.append(optimize.fmin(f,
         x0[i],xtol=1e-8,disp=0))
    self.atom = self.atom + [self.atom[1]+np.array([-1,1]),
    self.atom[0]+np.array([1,1]),
       self.atom[0]+np.array([0,2]),
       self.atom[1]+np.array([0,2])]

  # Measure potential amplitude on paths linking the minima
  def barrier(self, x1, x2):
```

```
    ppot = lambda x: self.potential(x1[0]+x*(x2[0]-x1[0]),
        x1[1]+x*(x2[1]-x1[1]))
    npot = lambda x: -ppot(x)
    xmin = optimize.fmin(ppot,0,xtol=1e-8,disp=0)[0]
    vmin = ppot(xmin)
    xmax = optimize.fmin(npot,0.5,xtol=1e-8,disp=0)[0]
    vmax = ppot(xmax)
    return vmax-vmin

  # Estimate the tunnel effect between x1 and x2
  # (very crappily, the point being to get an idea of the
      relative
  # between all tunnel effects)
  def tunnel(self, x1, x2):
    v = self.barrier(x1,x2)
    a = distance(x1,x2)
    return (np.exp(-a))/v

  # Returns estimations of tunnel effects between sites
  def tunnels(self):
    return
        np.array([self.tunnel(self.atom[0],self.atom[1]),
      self.tunnel(self.atom[0],self.atom[2]),
      self.tunnel(self.atom[1],self.atom[3]),
      self.tunnel(self.atom[2],self.atom[3]),
      self.tunnel(self.atom[1],self.atom[2]),
      self.tunnel(self.atom[0],self.atom[3]),
      self.tunnel(self.atom[0],self.atom[4])])

  # Plot potential landscape sections of potential along
      some
  # relevant segments, if 'show_sections' is not set to 0
  def draw(self, show_bonds=True, show_diagonals=True,
      show_sections=True, save=False):
    fig = plt.figure(figsize=(6,6))
    fig.canvas.set_window_title('Potential')
    # Contour plot
    n_points = 150
    x = np.linspace(-2.0, 2.0, n_points)
    if (not show_bonds):
      dy = 0.
```

```
else:
  dy= 1.
y = np.linspace(-2.0+dy, 2.0+dy, n_points)
X, Y = np.meshgrid(x, y)
plt.xlabel('x')
plt.ylabel('y')
plt.contourf(X, Y, self.potential(X,Y), 20)

if show_diagonals:
  link = [(0,1),(0,2),(1,3),(2,3),(1,2),(0,3),(0,4),
    (4,5),(3,5),(2,4),(3,4),(2,5),(1,5)]
  col = ['b','r','g','m','c','orange','gold',
    'b','r','g','c','orange','gold']
else:
  link = [(0,1),(1,3),(3,5),(5,4),(4,2),(2,0)]
  col = ['b','g','r','b','g','r']

# Draw the bonds along which the sections will be
   plotted
if show_bonds:
  for n in range(len(link)):
    x1 = self.atom[link[n][0]][0]
    x2 = self.atom[link[n][1]][0]
    y1 = self.atom[link[n][0]][1]
    y2 = self.atom[link[n][1]][1]
    plt.plot([x1,x2], [y1,y2], col[n])

plt.axis('scaled')
#~ plt.xlim([-0.5, 0.5])
#~ plt.ylim([-0.5, 0.5])

# Save a picture of the potential
if save:
  self.save_figure("Potential")

# Plot sections of the potential
if show_sections:
  fig = plt.figure()
  fig.canvas.set_window_title('Potential sections')
  plt.xlabel('Arb. units')
  plt.ylabel('Potential (Er)')
```

```
        n_points = 100
        A = np.linspace(0, 1, n_points)
        if show_diagonals:
          bonds = range(7)
        else:
          bonds = range(3)
        for n in bonds:
          x1 = self.atom[link[n][0]][0]
          x2 = self.atom[link[n][1]][0]
          y1 = self.atom[link[n][0]][1]
          y2 = self.atom[link[n][1]][1]
          dx = (x2-x1)/n_points
          dy = (y2-y1)/n_points
          z = []
          for i in range(n_points):
            z.append(self.potential(x1+i*dx,y1+i*dy))
          plt.plot(A,z,col[n])
          if save:
            self.save_figure("Sections")


class PotentialImpact(Potential):


  def __init__(self, A1, A2, A3, A4, A5, A6, phi):

    self.A1 = A1 #using everything in Hz
    self.A2 = A2
    self.A3 = A3
    self.A4 = A4
    self.A5 = A5
    self.A6 = A6
            self.phi = phi

  # Potential at point (x,y) (in lattice units)
  def potential(self, x, y):

    return (self.A1*np.cos(2*pi*y+self.phi)*
        np.cos(-np.sqrt(3)*pi*x+pi*y)+ #pumpcav1
            self.A2*np.cos(2*pi*y+self.phi)*
            np.cos(np.sqrt(3)*pi*x+pi*y)+ #pumpcav2
```

```
            self.A3*np.cos(-np.sqrt(3)*pi*x+pi*y)*
            np.cos(np.sqrt(3)*pi*x+pi*y)+ #cav1cav2
            self.A4*np.cos(2*pi*y+self.phi)**2+ #pump alone
            self.A5*np.cos((-np.sqrt(3)*pi*x)
            +(pi*y))**2+ #cav1
            self.A6*np.cos(np.sqrt(3)*pi*x+pi*y)**2
              #cav2
        )

# Hamiltonian
    def ham(self, n0, p1, p2):

            n0 = 5
            N = 2*n0+1
            #A1,A2,A3,A4,A5,A6,phi = (0,0,0,0,0,0,0)
            A1,A2,A3,A4,A5,A6,phi = (11.310, 11.310, 2.040,
                31.416, 1.020, 1.020, 0)
            K1=np.array([-np.sqrt(3.)/2,1./2])
            K2=np.array([0,1])

            H=np.zeros((N,N,N,N),'complex')
            q1,q2,q3,q4=np.indices(H.shape)

            #kinetic term
            H += np.where((q1==q3) & (q2==q4),
                (p1+(q1-n0))**2+
            (p2+(q2-n0))**2+2*np.dot(K1,K2)*(p1+(q1-n0))*(p2+(q2-n0)),
                0)

            #pump-cav1
            H += np.where((q3-q1==1) & (q4-q2==1),
                A1*0.25*np.exp(1j*phi),0)
            H += np.where((q3-q1==1) & (q4-q2==-1),
                A1*0.25*np.exp(1j*phi),0)
            H += np.where((q3-q1==-1) & (q4-q2==1) ,
                A1*0.25*np.exp(-1j*phi),0)
            H += np.where((q3-q1==-1) & (q4-q2==-1) ,
                A1*0.25*np.exp(-1j*phi),0)

            #pump-cav2
            H += np.where((q3==q1) & (q4-q2==1),
```

```
    A2*0.25*np.exp(1j*phi),0)
H += np.where((q3==q1) & (q4-q2==-1),
    A2*0.25*np.exp(-1j*phi),0)
H += np.where((q3-q1==2) & (q4-q2==-1),
    A2*0.25*np.exp(1j*phi),0)
H += np.where((q3-q1==-2) & (q4-q2==1),
    A2*0.25*np.exp(-1j*phi),0)

#cav1-cav2
H += np.where((q3-q1==1) & (q4==q2), A3*0.25,0)
H += np.where((q3-q1==-1) & (q4==q2), A3*0.25,0)
H += np.where((q3-q1==1) & (q4-q2==-2),
    A3*0.25,0)
H += np.where((q3-q1==-1) & (q4-q2==2),
    A3*0.25,0)


#pump
H += np.where((q3-q1==2) & (q4==q2),
    A4*0.25*np.exp(2*1j*phi),0)
H += np.where((q3-q1==-2) & (q4==q2),
    A4*0.25*np.exp(-2*1j*phi),0)
 H += np.where((q3==q1) & (q4==q2), A4*0.25*2,0)


#cav1
H += np.where((q3==q1) & (q4-q2==2), A5*0.25,0)
H += np.where((q3==q1) & (q4-q2==-2), A5*0.25,0)
H += np.where((q3==q1) & (q4==q2), A5*0.25*2,0)


#cav2
H += np.where((q3-q1==2) & (q4-q2==-2),
    A6*0.25,0)
H += np.where((q3-q1==-2) & (q4-q2==2),
    A6*0.25,0)
H += np.where((q3==q1) & (q4==q2), A6*0.25*2,0)


return H
```

```
      def get_symmetry(self):
         return 0
```

```
#!/usr/bin/python
# -*- coding: utf8 -*-
# since this is imported everywhere, try to keep away from
   single-letter
# variables, especially e, i, j...

from math import pi
import numpy as np

#! Units and constants
#!--------------------
#! in S.I units (kg m s C)
#!
#! length: Bohr radius (m)
a0=5.291772108e-11
#! electron mass (kg)
me=9.10938188e-31
#! angular momentum: hbar
hbar=1.05457168e-34
h = 2*pi*hbar
hplanck = h
#! charge: e (C)
qe=1.60217653e-19
#! electrostatic force: 1/(4 pi e0)
Fe=8.9875516e9
#! Dielectric constant (F m^-1)
eps0=8.854187817e-12
#! Hartree energy: e^2/(4 pi e0 a0) = (hbar/a0)**2/me
E0=4.35974417e-18
#! Boltzman constant
kb=1.3806504e-23
#! Atomic mass units (kg)
amu = 1.660538782e-27
#! Proton mass (kg)
mp = 1.67262171e-27
#! Avogadro constant (mol^-1)
NAvogadro = 6.02214179e23
#! Magnetic constant
```

```
mu0 = 4*pi*1e-7
#! Bohr magneton
muB = 9.27400915e-24
#! Nuclear magnetic moment
muN = 5.05078324e-27
#! Speed of light
c = 2.99792458e8
#! fine structure constant alpha (1)
alpha = 7.2973525376e-3
#! gravity
gravity = 9.81

#
m87Rb = 86.909180520*amu
m40K = 39.963999*amu
m6Li = 6.015*amu # Wiki (Jakob)
m133Cs = 132.905451931*amu
m23Na = 22.9897692807*amu

m ={}
m["K40"] = 39.963999*amu
m["Rb87"] = 86.909180520*amu
m["Cs133"] = 132.905451931*amu

#
lambda_yag = 1064e-9
#
k = 2*pi/lambda_yag
#
ER_40K = h**2/(2*m40K*lambda_yag**2)


####### parameters for IMPACT experiment #######

lambda_impact = 785.3e-9 #wavelength
k_imp = 2*pi/lambda_impact
ER_87Rb = h**2/(2*m87Rb*lambda_impact**2) #recoil energy
omegarec = ER_87Rb/hbar #recoil frequency


#experimental parameters
```

```
g1 = 2*pi*1.8e6 #cavity couplings in Hertz
g2 = 2*pi*1.8e6
alph1 = 10 #coherent state amplitude
alph2 = np.sqrt(200-alph1**2)
Omegap = 2*pi*100e6 #transverse pumo frequency
Deltaa = 2*pi*2e12 #detuning

eta1 = Omegap*g1/Deltaa
eta2 = Omegap*g2/Deltaa
eta3 = g2*g1/Deltaa
Up = Omegap**2/Deltaa
U1 = g1**2/Deltaa
U2 = g2**2/Deltaa

#coefficients
A1 = hbar*eta1*(2*alph1)
A2 = hbar*eta2*(2*alph2)
A3 = (alph1*alph2+alph2*alph1)*hbar*eta3
A4 = hbar*Up
A5 = hbar*U1*(alph1**2)
A6 = hbar*U2*(alph2**2)

#coefficient in units of recoil energy to be used in the
    main code
print A1/ER_87Rb
print A2/ER_87Rb
print A3/ER_87Rb
print A4/ER_87Rb
print A5/ER_87Rb
print A6/ER_87Rb
```

List of Figures

Bibliography

[1] T. Esslinger and T. Donner et al. Quantum phases from competing short- and long-range interactions in an optical lattice. *Nature*, 532:476–479, 2016.

[2] M. Greiner et al. Collapse and revival of the matter wave field of a bose-einstein condensate. *Nature*, 419, 2002.

[3] J. Leonard, A. Morales, P. Zupancic, T. Esslinger, and T. Donner. Supersolid formation in a quantum gas breaking continuous translational symmetry. *arXiv*, 2016.

[4] Richard P. Feynman. Simulating physics with computers. *International Journal of Theoretical Physics*, 21, 1982.

[5] Seth Lloyd. Universal quantum simulators. *Science*, 273(5278):1073–1078, 1996.

[6] G. Brumfiel. Quantum leaps. *Nature editorial*, 491:322, 2012.

[7] T. Johnson, S. Clark, and D. Jaksch. What is a quantum simulator. *EPJ Quantum Technology*, 2014.

[8] T. Schaetz, C. Monroe, and T. Esslinger. Focus on quantum simulation. *New J. Phys.*, 15:1073–1078, 2013.

[9] H. Moritz et al. Exciting collective oscillations in a trapped 1d gas. *PRL*, 91(250402), 2013.

[10] Z. Hadzibabic et al. Quantum gases: The cold reality of exclusion. *Nature Physics*, 6, 2010.

[11] H. Shiba and Y. Kuramoto. Special topics: Kondo effect ? 40 years after the discovery of kondo effect. *J. Phys. Soc. Jpn.*, 74, 2005.

[12] D. Jaksch and P. Zoller. The cold atom hubbard toolbox. *Annals of Physics*, 315, 2005.

[13] G. Roati et al. Anderson localization of a non-interacting bose-einstein condensate. *Nature*, 2008.

[14] C. Nayak et al. Non-abelian anyons and topological quantum computation. *Rev. Mod. Phys.*, 80, 2008.

[15] M. Leweinstein, V. Ahufinger, and A. Sampera. *Ultracold atoms in optical lattices, simulating quantum many body systems*. Oxford University Press, 2012.

[16] I Bloch, Dalibard J., and Nascimbène S. Quantum simulations with ultracold quantum gases. *Nature*, 8, 2012.

[17] W. Phillips. Laser cooling and trapping of neutral atoms - nobel lecture. *Nobel lecture*, 1997.

[18] W. Ketterle. When atoms behave as waves: Bose-einstein condensation and the atom laser. *Nobel lecture*, 2001.

[19] W. Ketterle, D. Durfee, and D-M. Stamper-Kurn. Making, probing and understanding bose-einstein condensates. *ArXiv*, 1999.

[20] I. Cirac and P. Zoller. Goals and opportunities in quantum simulation. *Nature Physics*, 8, 2012.

[21] H. Ritsch, P. Domokos, F. Brenneke, and T. Esslinger. Cold atoms in cavity generated dynamical optical potentials. *Reviews of Modern Physics*, 85, 2013.

[22] H. Ritsch, C. Maschler, and I. Mekhov. Ultracold atoms in optical lattices generated by quantized light fields. *Eur. Phys. J.*, 85, 2008.

[23] F. Brenneke et al. Qed with a bose einstein condensate. *Nature*, 450, 2007.

[24] C. Cohen-Tannoudji, J. Dupont-Roc, and G. Grynberg. *Atom - Photon Interactions: Basic Process and Appilcations*. Wiley, 1998.

[25] S. Huber. Experimental and theoretical aspects of quantum gases, lecture notes. 2015.

[26] F. Brenneke et al. Cavity opto-mechanics with a bose-einstein condensate. *Science*, 322, 2008.

[27] J. Klinder, H. Keßler, M. Bakhtiari, M. Thorwart, and A. Hemmerich. Observation of a superradiant mott insulator in the dicke-hubbard model. *PRL*, 115, 2015.

[28] Y. Colombe et al. Strong atom?field coupling for bose?einstein condensates in an optical cavity on a chip. *Nature*, 450, 2007.

[29] K. Baumann, C. Guerlin, F. Brennecke, and T. Esslinger. Dicke quantum phase transition with a superfluid gas in an optical cavity. *Nature*, 464, 2010.

[30] P. Domokos and H. Ritsch. Mechanical effects of light in optical resonators. *J. Opt. Soc.*, 20(5), 2003.

[31] T. Donner, S. Huber, D. Nishant, and F. Brenneke. Phase transitions in a bose-hubbard model with cavity-mediated global-range interactions. *arXiv*, 2016.

[32] J. Wen, Y. Zhang, and M. Xiao. The talbot effect: recent advances in classical optics, nonlinear optics, and quantum optics. *Advances in Optics and Photonics*, 5:83–130, 2013.

[33] M. V. Berry et al. Quantum carpets, carpets of light. *Physics World*, 14(6):39–44, 2001.

[34] J. Eberly et al. Periodic spontaneous collapse and revival in a simple quantum model. *PRL*, 44(20), 1980.

[35] M. Lewenstein and L. You. Quantum phase diffusion of a bose-einstein condensate. *PRL*, 77, 1996.

[36] A. Imamoglu, M. Lewenstein, and L. You. Inhibition of coherence in trapped bose-einstein condensates. *PRL*, 78, 1997.

[37] E.M. Wright et al. Collapses and revivals of bose-einstein condensates formed in small atomic samples. *PRL*, 77, 1996.

[38] W. Ketterle et al. Bose-einstein condensation in a gas of sodium atoms. *PRL*, 75(22), 1995.

[39] M. Nakano et al. Quantum-phase dynamics of two-component bose einstein condensates: Collapse revival of macroscopic superposition states. *Physica B*, 370(1-4), 2005.

[40] J. H. Huckans et al. Quantum and classical dynamics of a bec in a large-period optical lattice. *arXiv*, 2009.

[41] H. Veksler and S. Fishman. Collapses and revivals of matter waves. *arXiv*, 2015.

[42] Markus Greiner. *Ultracold quantum gases in three-dimensional optical lattice potentials*. PhD thesis, LMU, 2003.

[43] Roy J Glauber. *Quantum theory of optical coherence*. John Wiley & Sons, 1963.

[44] C. Straatsma and E. Cornell et al. Collapse and revival of the monopole mode of a degenerate bose gas in an isotropic harmonic trap. *ArXiv*, 2016.

[45] M. Kaur, B. Arora, and Arvind. Effect of dissipative environment on collapses and revivals of a nonlinear quantum oscillator. *ArXiv*, 2016.

[46] Pimenta H. and D. James. A characteristic function approach to the jaynes-cummings model revivals. *ArXiv*, 2016.

[47] Singleton J. *Band theory and electronic properties of solids*. Oxford University Press, 2013.

[48] C. Kittel. *Introduction to solid state physics*. Oxford University Press, 1966.

[49] S. Simon. *The Oxford Solid State Basis*. Oxford University Press, 2001.

[50] M. Afzelius, N. Gisin, and H. de Riedmatten. Quantum memories for photons. *Physics Today*, 68, 2015.

[51] M. Afzelius et al. Demonstration of atomic frequency comb memory for light with spin-wave storage. *Physical Review Letters*, 104, 2010.

[52] Eric D. Black. An introduction to pound?drever?hall laser frequency stabilization. *Am. J. Phys.*, 69, 2001.